DYNAMICS OF CABLES SUBJECTED TO SHEAR CURRENT EXCITATION

by

Christopher T. Howell

Bachelor of Science, Texas A&M University

SUBMITTED TO THE DEPARTMENT OF OCEAN ENGINEERING IN PARTIAL FULFILLMENT OF THE REQUIREMENTS FOR THE DEGREE OF

MASTER OF SCIENCE IN OCEAN ENGINEERING

at the

MASSACHUSETTS INSTITUTE OF TECHNOLOGY

September 1989

Signature of Author _____
Department of Ocean Engineering
September 31, 1989

Certified by _____
Professor Michael S. Triantafyllou
Thesis Supervisor

Accepted by _____
Professor A. Douglas Carmichael
Chairman, Graduate Thesis Committee

DYNAMICS OF CABLES SUBJECTED TO SHEAR CURRENT EXCITATION

by

Christopher T. Howell

Submitted to the Department of Ocean Engineering on September 31, 1989 in partial fulfillment of the requirements for the degree of Master of Science in Ocean Engineering.

Abstract

The goal of this research was to gain a better understanding of the effects of a variable current profile on the dynamics of long cables. Full-scale experimental results have shown motion amplitude modulation with time and depth. Research was aimed at the development of a numerical model capable of predicting motions of this type given a shear current excitation. The model is based on solution of the taut string equation using a Green's function approach with infinite cable boundary conditions. In the method, excitation forces are correlated over discrete regions and phase shifts between regions are accomplished with random phase angles.

A spectral analysis of full-scale experimental data was conducted to determine the motion characteristics of a towed cable in a sheared current. Homomorphic processing and the so-called "envelope approach" were implemented to aid in the determination of the strumming and beating frequencies.

The numerical results obtained supported the experimental data as amplitude modulation was prevalent at discrete points through time. A dependence on correlation length was shown while damping also proved to be of importance. Homomorphic processing and the envelope approach both proved to be effective tools as beating and strumming frequencies were more readily identified with their use.

Thesis Supervisor: Professor Michael S. Triantafyllou
Title: Associate Professor of Ocean Engineering

Dedication

To my advisor Micheal S. Triantafyllou for his efforts in this research. Through his guidence and push this work was completed.

To Mark A. Grosenbough for his insights on this project, especially in the frequency analysis portion of the research.

To Mike Drooker for his beyond the call of duty help in the design lab.

To the Office of Naval Research for the financial support that has made my advance studies possible.

And finally to my parents. All they ever asked was that I make them proud.

Table of Contents

Abstract 2
Dedication 3
Table of Contents 4
List of Figures 5
List of Tables 6

1. Introduction 7

2. Fundamentals of Flow Induced Vibrations 9
2.1 Vortices 9
2.2 Lift and Drag Forces 11
2.3 Correlation Length 12

3. Investigation of Shear Current Loading 14
3.1 Previous Research 14
3.2 Analytic Method of Approach 15
3.2.1 Governing Equation 16
3.2.2 Mathematical Model 16
3.2.3 Green's Function Solution 19

4. Numerical Results 22
4.1 Two-Point Excitation 22
4.2 Uniform Current Excitation 25
4.3 Shear Current Excitation 27
4.3.1 Exact Solution of Analytic Equation 27
4.3.2 Discrete Solution 29

5. Spectral Analysis of Full-Scale Experimental Data 43
5.1 Discussion of Experiment 43
5.2 Data Analysis Procedure 47
5.2.1 Characteristics of Raw Data 47
5.2.2 Homomorphic Processing 48
5.2.3 Envelope Approach 50
5.2.4 Power Spectrum Calculation 50
5.2.5 Example Analysis 53
5.3 Presentation of Results 53
5.4 Discussion of Results 58

6. Conclusions and Recommendations 68

List of Figures

Figure 2-1: Example of vortex shedding behind a circular cylinder 2.1
Figure 3-1: Definition of problem parameters 3.2.1
Figure 3-2: Variable lift coefficient model 3.2.2
Figure 4-1: Description of two point excitation problem 4.1
Figure 4-2: Time series for cable excited at two points. Excitation frequency of 8.75π rad/sec at both points 4.1
Figure 4-3: Time series for cable excited at two points. Excitation frequencies of 8.5π and 9π rad/sec. 4.1
Figure 4-4: Time series for cable in a uniform current field 4.2
Figure 4-5: Fluid velocity profile for case #1 4.3.2
Figure 4-6: Time series records for case #1 excitation profile. 4.3.2
Figure 4-7: Longer time series records for case #1 current profile 4.3.2
Figure 4-8: Fluid velocity profile for case #2 4.3.2
Figure 4-9: Time series records for case #2 excitation profile 4.3.2
Figure 4-10: Fluid velocity profile for case #3 4.3.2
Figure 4-11: Time series records for case #3 excitation profile 4.3.2
Figure 4-12: Effect of decreased correlation length on vibrations of cable midpoint excited by case #1 current profile 4.3.2
Figure 4-13: Comparison of various bracket regions for randomized excitation forces. 4.3.2
Figure 4-14: Comparison of results for various damping coefficients. 4.3.2
Figure 4-15: Cable shape and associated displacement envelope used for variable lift coefficient model 4.3.2
Figure 5-1: Typical setup for full-scale experiment 5.1
Figure 5-2: Ship course track and current direction for run #4 5.1
Figure 5-3: Typical current profile for test run #4 5.1
Figure 5-4: Canonic representation of homomorphic system 5.2.2
Figure 5-5: Power spectrum for unprocessed signal 5.2.5
Figure 5-6: Power spectrum after homomorphic processing 5.2.5
Figure 5-7: Power spectrum for envelope of original signal 5.2.5
Figure 5-8: Unprocessed power spectra for channel 0 data sets 5.3
Figure 5-9: Unprocessed and processed power spectra for instrument bottle A 5.3
Figure 5-10: Unprocessed and processed power spectra for instrument bottle B 5.3
Figure 5-11: Unprocessed and processed power spectra for instrument bottle C 5.3
Figure 5-12: Unprocessed and processed power spectra for instrument bottle D 5.3
Figure 5-13: Unprocessed and processed power spectra for instrument bottle E 5.3
Figure 5-14: Variation of strumming and beating frequencies with depth 5.4

List of Tables

Table 5-I: Characteristics of cable used in the experiment 5.1
Table 5-II: Spectral peaks as determined from the spectral analysis 5.3
Table 5-III: Estimates of strumming and beating frequencies at discrete points along the cable 5.3

Chapter 1

Introduction

The study of flow induced vibrations of long cables has been the subject of much interest with the advent of deep ocean towed systems, such as the ARGO/JASON system developed at the Woods Hole Oceanographic Institute. The basic problem is that without a thorough understanding of the cable dynamics involved, it is very difficult to accurately predict the location of the system, relative to the ship, once the system is launched. The complexity stems from the fact that the exciting forces are predominantly due to nonlinear drag. The cable motions transverse to the incident flow are of great importance as they tend to increase the magnitude of the drag force by increasing the apparent projected area of the cable.

As a viscous fluid passes over a bluff body, the flow will begin to separate or detach from the body. This separation gives rise to the formation of vortices which, in turn, create lift forces which act transverse to the flow. The magnitude and frequency of these forces are related to the component of the incoming flow velocity normal to the body. Therefore, when considering a velocity profile which varies with depth, i.e. a shear current, the excitation will vary in magnitude and frequency along the length of the cable. In addition, the phase of the lift forces are also subject to change along the cable. The net effect on transverse cable motions is the subject of this research.

Laboratory experiments do not provide a good basis for investigating problems of this nature. The reason is that it is virtually impossible to adequately model both the flow environment and the cable system when dealing with the cable length to diameter ratios desired. The large ratios that are required yield extremely small experimental diameters

(typically less than one mm). Therefore, numerical predictions and full-scale experiments are sought. Both avenues have been persued in this research.

Previous full-scale experimental results have shown motion amplitude modulation with time and depth [2]. This research was aimed at developing a numerical model capable of predicting how a long cable responds to a shear current excitation. The model is based on a Green's function solution of the damped taut string equation for a constant tension cable of infinite length. In addition to the theoretical studies, a spectral analysis of full-scale experimental data was conducted to determine the nature of the measured cable vibrations. Homomorphic processing and the so-called "envelope approach" were implemented to aid in the determination of the vibration frequencies.

Chapter 2

Fundamentals of Flow Induced Vibrations

Flow induced vibrations have been studied extensively in the past. However, the complexity of the problem has left many questions still unanswered. The phenomenon of vortex shedding gives rise to high frequency lift forces which act transverse to the flow. If the structure is allowed to move, the resulting transverse motions can act to increase the in-line drag force by a factor of up to 2.3 times the stationary structure values [9]. Structural failure due to fatigue is also a concern.

2.1 Vortices

In order to study the nature of flow induced cable vibrations it is necessary to understand the excitation forces. When a real fluid flows over a body the viscous effects are confined to a small region surrounding the body. This region is called the boundary layer. The flow velocity increases across the boundary layer, with particles on the body surface remaining motionless. The net effect is that the fluid particles will begin to acquire some vorticity. As the fluid flows past the body, an inverse pressure gradient will act to decelerate the flow. For bluff bodies, such as circular cylinders, this deceleration is so strong that there is not enough time to spread the vorticity out, causing the flow to separate from the body. This results in the shedding of vortices. The vortex shedding process is strongly dependent on the Reynolds number, where R_n is defined as

$$R_n = \frac{U_n D}{\nu} \tag{2.1}$$

where

U_n = normal velocity component

D = cable diameter

ν = kinematic viscosity

In turbulent flow there is a greater intermixing between fluid layers. This enables the vorticity to be spread more readily, causing the separation point to move further downstream on the body. Numerous sources show the flow patterns for various Reynolds numbers and should be consulted if additional information is sought (see [8]). Reynolds numbers greater than 10^4 but below 3×10^5 are typical of the problem under investigation.

For very low Reynolds numbers, less than 40, symmetric attached vortices are formed behind the body. However, as the Reynolds number is increased, instabilities in the flow cause an asymmetric shedding pattern to develop. The resulting flow pattern is shown in figure 2.1. This pattern is known as the Von Karman vortex street.

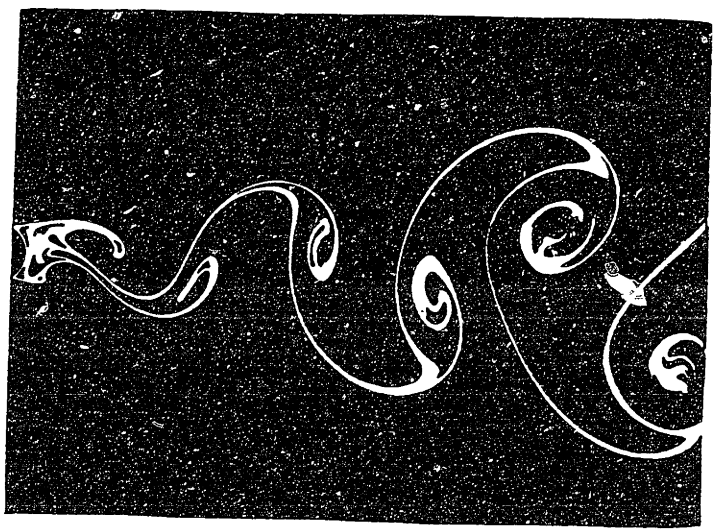

Figure 2-1: Example of vortex shedding behind a circular cylinder

The frequency of vortex shedding is given by the Strouhal relation. The Strouhal number S_t is defined as

$$S_t = \frac{f_s D}{U_n} \tag{2.2}$$

where

f_s = vortex shedding frequency

Two vortices, one from each side, are shed during one period. Experiments show that for a wide range of Reynolds numbers the Strouhal number remains constant at a value of roughly 0.2 [8].

2.2 Lift and Drag Forces

As the vortices are shed from the body, the higher velocities they create give rise to a transverse pressure gradient. This pressure gradient results in a lift force which acts in the direction away from the last shed vortex. The frequency of this lift force is the same as the shedding frequency. Therefore, the Strouhal relation can be used to determine the excitation frequency from the fluid velocity.

The magnitude of the lift force is a function of the square of the normal component of the free stream velocity and is Reynolds number dependent. Experiments have shown that the magnitude of the lift force decays as the cable displaces a significant distance from its mean position, dropping to zero when the motion amplitude is greater than one diameter [8]. Therefore, the transverse motions are self limited in nature. The surface roughness can also effect the lift force. Higher lift coefficients are associated with roughened cylinders [8].

In addition to the lift forces, in-line drag forces at twice the shedding frequency occur. However the magnitude of the resulting oscillations are relatively small [8]. More

importantly, the transverse cable motions act to increase the apparent projected area of the cable, thus increasing the total in-line drag force. An estimate of the maximum drag force that may occur can be computed using a projected area that is increased by twice the motion amplitude [3]. This does not mean, however, that such a large drag force is always realized (frequency, for example, has a significant effect).

2.3 Correlation Length

The spanwise correlation of the vortex sheet can greatly affect the structural response. The spanwise correlation describes how well the phase angles of the lift forces are correlated along the length of the cable. Partial spanwise correlation leads to variations in both the frequency and amplitude of the lift forces [8]. Experiments have shown that for stationary cylinders, the correlation length is Reynolds number dependent and is typically on the order of one diameter for the problem of interest. However, lateral vibrations of the cable will serve to correlate the phase of the shedding [8]. This is true for even small transverse oscillations. To what extent the correlation length is increased is not fully known. In addition, little or no information is available on correlation lengths in shear flows.

As the Strouhal frequency approaches the natural frequency of the system, the characteristics of the shedding process begin to change and the shedding frequency will collapse or "lock in" to the structural frequency. That is, the resonance vibrations begin to control the shedding process thereby exciting the structure at its own natural frequency. This phenomenon, sometimes called lock in, can encompass ± 25 to 30% of the vortex shedding frequency and can cause large amplitude motions [8]. Koopman has shown that lock in can cause an increase in the correlation length [5]. Why this occurs is not fully

known. The low-order natural frequencies for long cables are typically much lower than the vortex shedding frequencies, so it is unlikely that the long cables will experience lock in over their entire length. However, it is possible to excite higher-order modes, causing lock in to occur over some localized distance.

Chapter 3

Investigation of Shear Current Loading

The effect of a nonuniform flow profile has not received nearly the attention given to the constant velocity case. This is unfortunate as actual ocean current profiles typically exhibit some shear. Even if the profile is uniform, shear-type excitation will occur if the cable is curved, as the component of the velocity normal to the cable will vary with depth.

The characteristics of the lift force will change considerably along the cable if the velocity profile is nonuniform. The first consequence is to change the magnitude of the force which, as stated earlier, is a function of the square of the inflow velocity. Secondly, the frequency of the excitation, given by the Strouhal relation, will also change with depth. The net effect on the cable motions is the subject of this research.

3.1 Previous Research

The research that has been conducted in the past has mainly been concerned with determining how shear currents affect the in-line drag. Experimental studies were conducted by Kim [4] to determine the shear effects on the vibration response of long cables. The data obtained showed that the average drag coefficient was lower than for a cable subjected to a uniform current, and was only 25% higher than for a stationary cylinder.

It is well known that the superposition of two traveling waves of different frequencies serves to create both slow and fast variations in displacement. The slowly varying amplitude modulation, sometimes called the beat phenomena, is demonstrated in many

fields of science. Engbretsen [2] demonstrated numerically that the effect of the frequency variation in shear flows is to create displacement amplitude modulations at discrete points along the cable. The magnitude of the resulting motions were shown to be smaller than for similar cases with a uniform current. Engbretsen's findings were supported by his analysis of full-scale experimental data, as the time records he presented demonstrated motion amplitude modulation which was directly attributable to a shear current excitation.

3.2 Analytic Method of Approach

Analytical studies were mainly concerned with the solution of the governing equation using a Green's function approach. Green's functions are commonly employed to solve linear boundary value problems. The power of the method lies in the fact that the Green's function is independent of the nonhomogeneous term in the governing differential equation. Thus, once the function is determined, the solution of the boundary value problem for different nonhomogeneous terms is obtained by a single integration.

The Green's function can be interpreted as the response of the system due to an applied point load, or Dirac-delta function, of density δ. The two point Green's function $G(x,y)$ describes the displacement at a point x due to a force at y. The total displacement of the system, caused by a loading distributed according to some function, can be determined at each point by integrating the Green's function over all possible points in the region of interest. This method lends itself to solving the problem at hand as the applied loading can be described as a set of locally acting excitations which are distributed along the cable.

3.2.1 Governing Equation

The governing equation for the transverse motions of a constant tension cable is given by equation 3.1.

$$m\frac{\partial^2 q}{\partial t^2} + b\frac{\partial q}{\partial t} = T\frac{\partial^2 q}{\partial x^2} \tag{3.1}$$

where

q = cable displacement

m = mass and added mass of the cable

b = damping constant

T = cable tension

This is known as the damped taut string equation and the parameters employed are more fully described in figure 3-1. As shown in this figure, a harmonic forcing function is applied at some distance y from the origin. The constant tension assumption greatly simplifies the analysis and previous findings show that its effects on the overall solution accuracy are minimal [2].

As the cable is displaced, displacement waves will develop which travel along the length of the cable. Experiments show that these waves are significantly attenuated due to hydrodynamic damping. Therefore there is virtually no reflection from the endpoints. For this reason, infinite cable boundary conditions are employed in this analysis. A segment within the cable can then be investigated with no interference arising from reflected waves.

3.2.2 Mathematical Model

In order to solve the problem at hand, the characteristics of the excitation forces must be modeled in some fashion. As stated earlier, the loading is caused by lift forces which

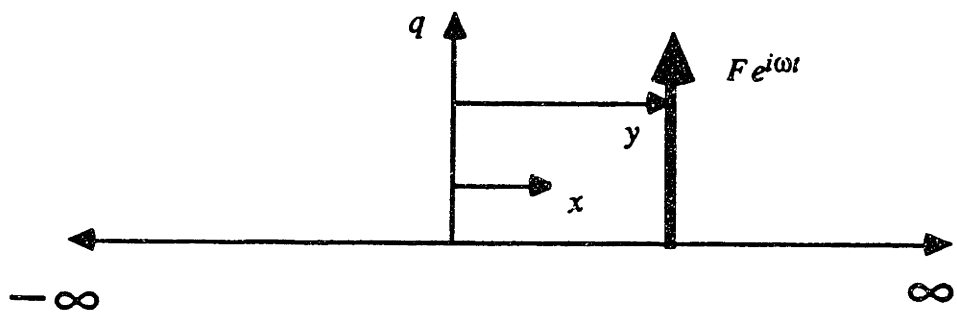

Figure 3-1: Definition of problem parameters

arise from vortex shedding. The frequency of these forces can be determined from the Strouhal relation, which is rewritten here in a slightly different form for completeness.

$$\omega(y) = \frac{2\pi U_n(y) S_t}{D} \tag{3.2}$$

The frequency ω and velocity U_n are written here as functions of y to reinforce this fact.

The magnitude of the lift force per unit length is determined by the semi-empirical equation given below.

$$F(y) = \frac{1}{2}\rho C_l D U_n^2(y)\, dl \tag{3.3}$$

where

ρ = fluid density

C_l = coefficient of lift

For this analysis a constant lift coefficient value of 0.6 was employed. In addition, a model using a coefficient, based on the displacement amplitude envelope, was also developed. The later model is used to account for the self limited nature of the cable vibrations. A linear variation with displacement, as shown in figure 3-2, was assumed for the coefficient.

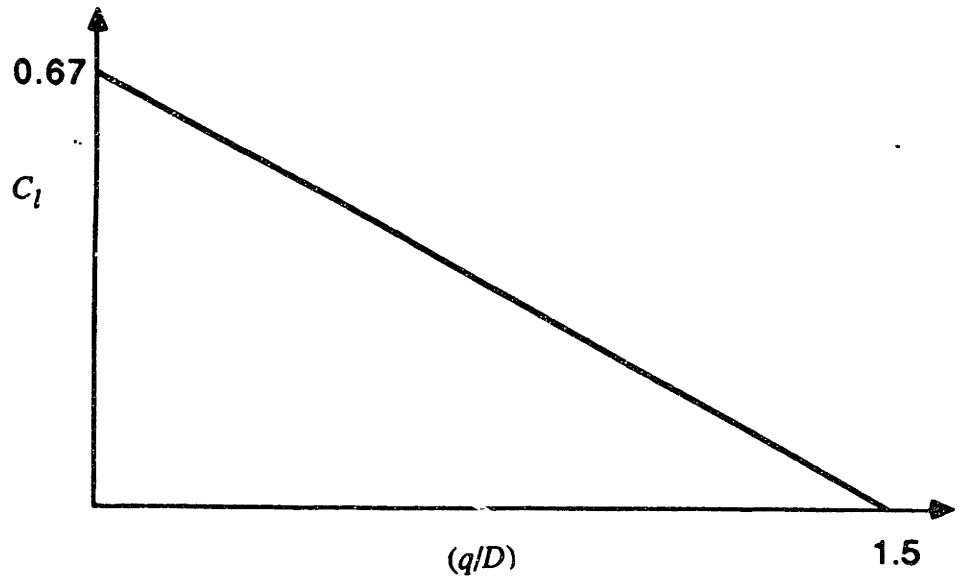

Figure 3-2: Variable lift coefficient model

The added mass of the cable was assumed to equal the mass of the fluid displaced by the cable. The damping was considered to be mainly hydrodynamic, and some manipulation of the damping term, as shown in the next section, was performed.

As mentioned earlier, the correlation length plays an important role in the analysis. To account for this, phase angles were used to correlate the excitation over some predetermined length. The magnitude of these angles are selected with random number generator.

3.2.3 Green's Function Solution

The first step in the solution process is to eliminate the time dependence in the response term by assuming a harmonic displacement. This can be written as follows:

$$q(x,t) = \bar{q}(x)e^{i\omega t} \tag{3.4}$$

As the cable is displaced at a specific point, displacement waves are generated. These waves travel away from the excitation. With this in mind, the $\bar{q}(x)$ function may be decomposed into two different wave forms, one valid on each side of the loading point. The form of these functions is shown below.

$$\bar{q}_l(x) = C_1 e^{ikx} \qquad -\infty < x \leq y \tag{3.5a}$$

$$\bar{q}_r(x) = C_2 e^{-ikx} \qquad y \leq x < \infty \tag{3.5b}$$

where

$$k(y) = \sqrt{m\omega^2(1-\beta i)/T}$$

$$\beta = \frac{b}{m\omega}$$

The damping term has been rewritten in this form to simplify the analysis. The term k is known as the wave number and β is the nondimensional damping parameter. Note that with damping the wave number k is complex.

There are two conditions which must be satisfied by equations 3.5a and b. First of all, the two functions must be equal at the point of excitation. This is to ensure continuity of the solution. Secondly, for equilibrium, the exciting force must be offset by the

transverse component of the tension. Mathematically the two conditions can be stated as follows:

$$\bar{q}_l(x) = \bar{q}_r(x) \qquad at \quad x=y \tag{3.6}$$

$$F = T\{\frac{\partial \bar{q}_r}{\partial x} - \frac{\partial \bar{q}_l}{\partial x}\} \qquad at \quad x=y \tag{3.7}$$

Solving the governing equation with these two conditions yields the solution for the displacement of the cable due to a point load, of magnitude F and frequency ω, located at y.

$$q_l(x,t) = \frac{Fi}{2Tk} e^{i\{wt+k(x-y)\}} \qquad -\infty < x \le y \tag{3.8a}$$

$$q_r(x,t) = \frac{Fi}{2Tk} e^{i\{wt-k(x-y)\}} \qquad y \le x < \infty \tag{3.8b}$$

The Green's function solution for a load distributed along the cable can be obtained by integrating equations 3.8a and b over their appropriate intervals.

$$q(x,t) = Re\{\frac{\rho C_l D i}{4T}(I_1 + I_2)\} \tag{3.11}$$

where

$$I_1 = \int_0^x \frac{U_n^2}{k} e^{i\{\omega t-k(x-y)+\phi\}}\, dy$$

$$I_2 = \int_x^L \frac{U_n^2}{k} e^{i\{\omega t+k(x-y)+\phi\}}\, dy$$

Equations 3.2 and 3.4 were implemented in the calculation of 3.11. The phase angle ϕ is used to specify the correlation length.

Equation 3.11 provides the basis with which the effects of a shear flow can be

studied. Further simplifications, as described in the next chapter, can be used to obtain exact solutions of this equation. For more complex cases, the trapezoidal rule was used to perform the necessary numerical integration.

Chapter 4

Numerical Results

The results of an analytic study of cable vibrations due to variable frequency excitation are presented in this chapter. A simple two-point excitation situation and several more advanced distributed loading models were investigated. The goal was to determine how relevant parameters, such as the excitation frequency gradient, effect the overall nature of the vibrations. Attempts were made to verify solutions when possible.

4.1 Two-Point Excitation

The vibration response of a cable subjected to a harmonic loading at two discrete points on the cable is discussed in this section. The problem is shown in figure 4-1. A solution was obtained by superimposing linear solutions of the form 3.8a and b. The solution is given by equation 4.1, where F_i and ω_i are the excitation magnitude and frequency at the point y_i, respectively, and all other variables are as defined previously.

$$q(x,t) = Re\{\frac{F_1 i}{2Tk_1}(e^{i(\omega_1 t - k_1(x-y_1))}) + \frac{F_2 i}{2Tk_2}(e^{i(\omega_2 t + k_2(x-y_2))})\} \quad y_1 \le x \le y_2 \qquad (4.1)$$

This expression can be rewritten as shown in equation 4.2. In this case the constants have been grouped in the term C and the excitation force has been expressed as a function of the square of the excitation frequency.

$$q(x,t) = Re\{Ci\omega_1 e^{i(\omega_1 t - k_1(x-y_1))}[(1+\frac{\omega_2}{\omega_1})e^{i(\delta\omega t + (k_1+k_2)x - C')}]\} \qquad (4.2)$$

where

$\delta\omega = \omega_2 - \omega_1$

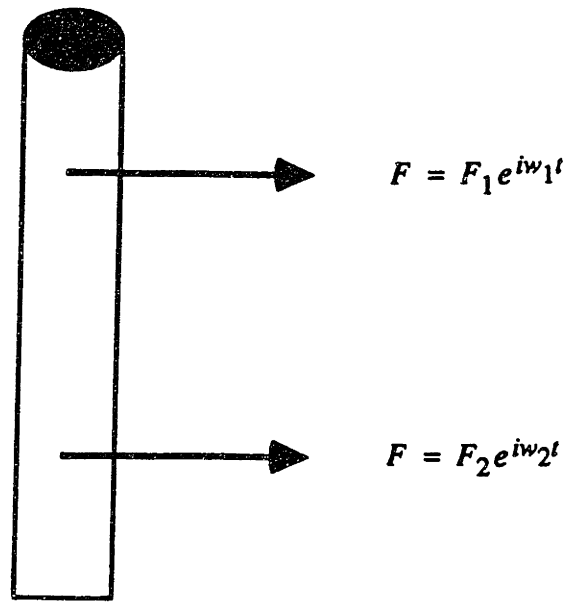

Figure 4-1: Description of two point excitation problem

$C' = k_1 y_1 + k_2 y_2$

The term in the brackets is known as the amplitude modulation factor and is slowly varying in both space and time. The difference frequency $\delta\omega$ represents the frequency of one beat in the time series. For this investigation, the beat frequency ω_b corresponds the time required for two beats to pass. It should be noted that this definition is somewhat different than the beat frequency denoted in most literature in that typically the difference frequency is called the beat frequency. To help eliminate confusion, the beat frequency shown in equation 4.3a will be called the "defined beat frequency". The strumming frequency ω_s describes the high frequency motions and is given as the average of the two exciting frequencies. Note that changing the location of the excitation forces alters C', effectively causing a phase shift in the time series.

$$\omega_b = \frac{\delta\omega}{2} \qquad (4.3a)$$

$$\omega_s = \frac{(\omega_2 + \omega_1)}{2} \tag{4.3b}$$

Two typical time series records are shown in figures 4-2 and 4-3. Figure 4-2 represents the situation where the two exciting frequencies are the same, namely 8.75π rad/sec. As readily seen, no amplitude modulation occurs. In contrast, exciting frequencies of 8.5π and 9.0π rad/sec were used to generate the time series in figure 4-3. This series clearly demonstrates periodic amplitude variation, or beats. The calculated beat period ($4\pi/\delta\omega$) of 8.0 sec can be visually confirmed and the frequency of the fast motion is given by the average of the two exciting frequencies. The visual findings are confirmed by a spectral analysis of the time series, as presented in Chapter 5.

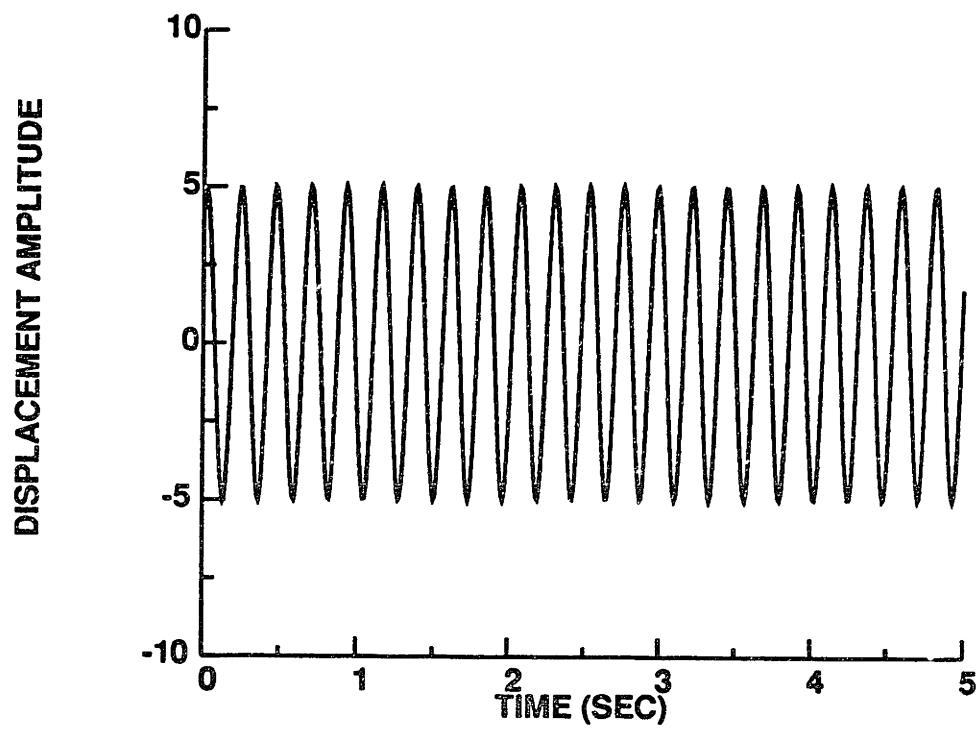

Figure 4-2: Time series for cable excited at two points. Excitation frequency of 8.75π rad/sec at both points

The effects of damping were investigated and the results showed that including

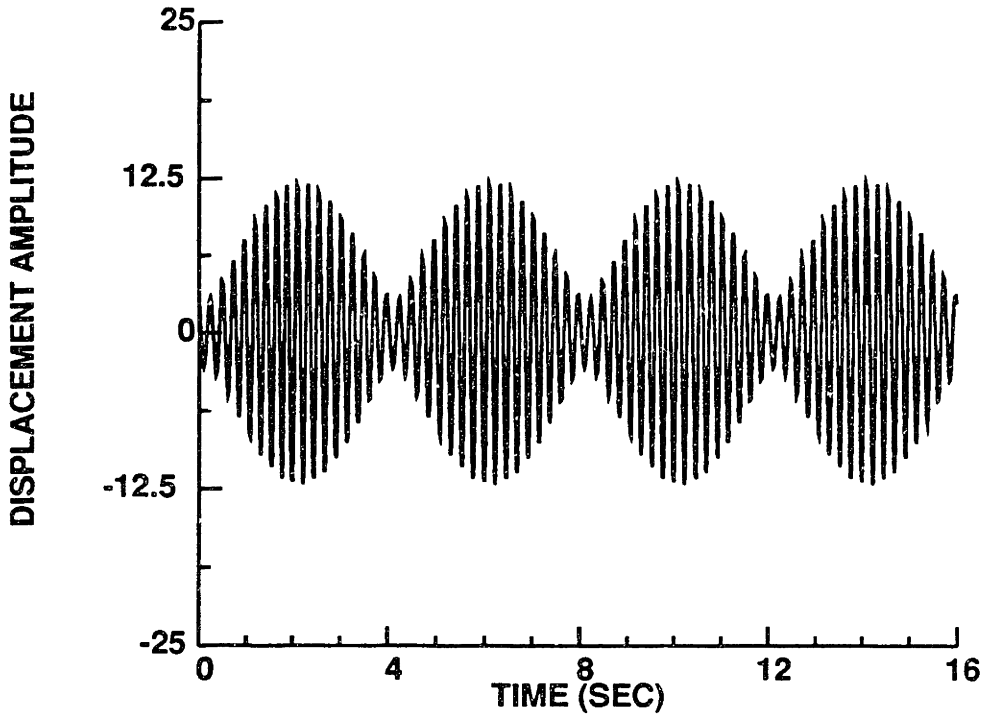

Figure 4-3: Time series for cable excited at two points. Excitation frequencies of 8.5π and 9π rad/sec.

damping serves to reduce the magnitude of the vibrations, while not altering the relevant vibration frequencies. These results provide backround with which the more detailed distributed loading case can be studied.

4.2 Uniform Current Excitation

The effect of a uniform current excitation was studied in two ways. The first method was by integrating equation 3.11 exactly. The second was with a numerical model called SCVP (Shear Current Vibration Predictor). This model uses the trapezoidal rule to solve equation 3.11 and incorporates phase angles to correlate the forces along the cable. The model is discussed in greater detail in section 4.2.2.

By assuming a constant velocity U_n, the problem is greatly simplified as the exciting frequency ω and the wave number k are no longer functions of distance along the cable. Solving equation 3.11, with zero phase angles, yields

$$q(x,t) = C e^{i\omega t}(2 - e^{-ikx} - e^{-ik(x-L)}) \qquad (4.4)$$

This equation shows that in a constant current, no amplitude modulation occurs. Equation 4.4 is represented by the time series in figure 4-4, for which a fluid velocity of 0.5 ft/sec and a damping coefficient β of 0.1 were used.

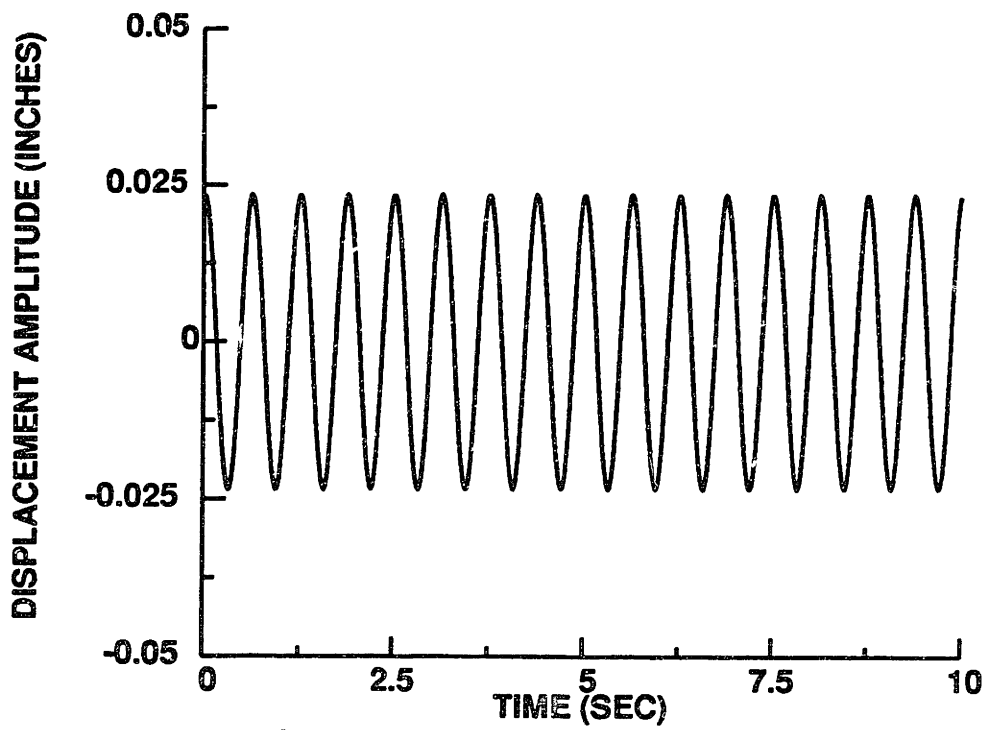

Figure 4-4: Time series for cable in a uniform current field

The results obtained from the model SCVP matched the analytic results exactly. This helped to verify the accuracy of the numerical procedure. Inclusion of the phase angles tended to alter the magnitude of the excitation as well as shift the time series along the time

axis. The vibration frequency, however, was not affected. These effects were determined to be strongly dependent on the magnitude of the phase angles as certain values increased the excitation while others caused a reduction in the vibration amplitude. Inclusion of damping reduced the vibrations.

4.3 Shear Current Excitation

The findings of the backround studies presented above provide insight into the distributed shear current loading problem. The complexity of equation 3.11 makes it very difficult to obtain closed form solutions. Nonetheless, by assuming a linearly varying profile, an exact analytic solution was derived. This result is discussed in the next section. In addition, the more flexible SCVP model was used to analyze a variety of flow fields. The effects of a variable lift coefficient, based on the cable displacement, and randomized lift force locations were also investigated with modified versions of the SCVP model.

4.3.1 Exact Solution of Analytic Equation

In order to validate the SCVP model, a closed form solution of equation 3.11 was sought. In the analysis, the random phase angles were eliminated and solutions were obtained both with and without damping. A linearly varying velocity profile was used to simplify the problem as much as possible. A considerable degree of algebra was involved which will not be shown here. The end result is shown in equation 4.4, where $f_i(x,t)$ represents a complicated function of space and time which is written in this form for simplicity.

$$q(x,t) = f_1(x,t) + f_2(x,t)\int_0^x e^{i(\alpha_2 y + \alpha_3 y^2)}dy + f_3(x,t)\int_x^L e^{-i(\alpha_5 y + \alpha_3 y^2)}dy \qquad (4.4)$$

where α_2 and α_5 are functions of x and t and α_3 is a constant, complex if damping is included. Solutions of the two integrals in equation 4.4 involves use of the complex error function, as shown below.

$$\int_0^x e^{i(\alpha_2 y + \alpha_3 y^2)} dy = f_4(x,t)\, erf\left[\sqrt{-i\alpha_3}\, y - \frac{i\alpha_2}{2\sqrt{-i\alpha_3}}\right]_0^x \tag{4.5a}$$

$$\int_x^L e^{-i(\alpha_5 y + \alpha_3 y^2)} dy = f_5(x,t)\, erf\left[\sqrt{i\alpha_3}\, y + \frac{i\alpha_5}{2\sqrt{i\alpha_3}}\right]_x^L \tag{4.5b}$$

The above solution was implemented in a numerical procedure which included a separate subroutine for calculating the complex error function values. The obtained results were quite surprising in that the solutions tended to become unbounded with time, regardless if damping was included. To investigate the stability of the solution, an asymptotic expansion of the error function in time was performed. The criteria which dictates the stability of the complex error function of z is [1]

$$\lim_{z\to\infty} erf(z) \to 1 \qquad if\ |arg(z)| < \frac{\pi}{4} \tag{4.6}$$

Expansion of the error functions in equations 4.5a and b shows that the criteria is not satisfied if damping is not included as $arg(z)$ is identically equal to $\pi/4$ for all time. Unfortunately, the inclusion of damping causes the argument of one of the error functions listed to increase beyond the limiting value. The degree of damping dictates which error function becomes unbounded. These findings are quite disheartening as an exact solution of the analytic equation does not prove useful. At this point in time, reasons for this behavior are not known.

4.3.2 Discrete Solution

The SCVP model provides a simple forum in which the effects of shear current excitation may be studied. As mentioned previously, the model implements the trapezoidal rule to solve equation 3.11. After specification of the system characteristics, i.e. cable diameter and length, the velocity profile is generated by specifying the profile inflection points and the associated fluid velocities. The velocity is assumed to vary linearly between these points and the model generates the velocity magnitude at predetermined points along the cable. The phase of the lift forces is correlated over a preselected length and the magnitude of the phase angles is chosen randomly. Output from the model includes both the cable configuration at specified times and the displacement time records for discrete points on the cable.

To insure sufficient convergence of the results, limits on the maximum allowable time step and spacing between discrete points were set. Results showed that satisfactory convergence was obtained if the two criteria listed below were met.

$$xdis \leq \frac{2\pi}{min[Re\{k(y)\}]} \tag{4.7a}$$

where

xdis = distance between cable nodal points

$$tstep \leq \frac{2\pi}{min[\omega(y)]} \tag{4.7b}$$

where

tstep = time increment between calculations

The first case studied was a linearly varying current as shown in figure 4-5. To gain a better understanding of the dynamics involved, no phase angles were used in this case.

That is, the correlation length spanned the entire cable. A 2000 ft cable was used with a damping coefficient β=0.1 and displacement time records were determined at three points on the cable. Specifically, these points correspond to the mid-point, quarter and three-quarter chord positions. The results are shown in figure 4-6. These results show conclusively that beating occurs in the continuous case as predicted from the two point excitation results in section 4.1. An analysis of these time series records shows that the strumming frequency ω_s, or the frequency of the fast motions, is given by the local excitation frequency. The frequency of one beat in the time series $\omega_b/2$ is given by the difference between the largest (top end) and local excitation frequencies.

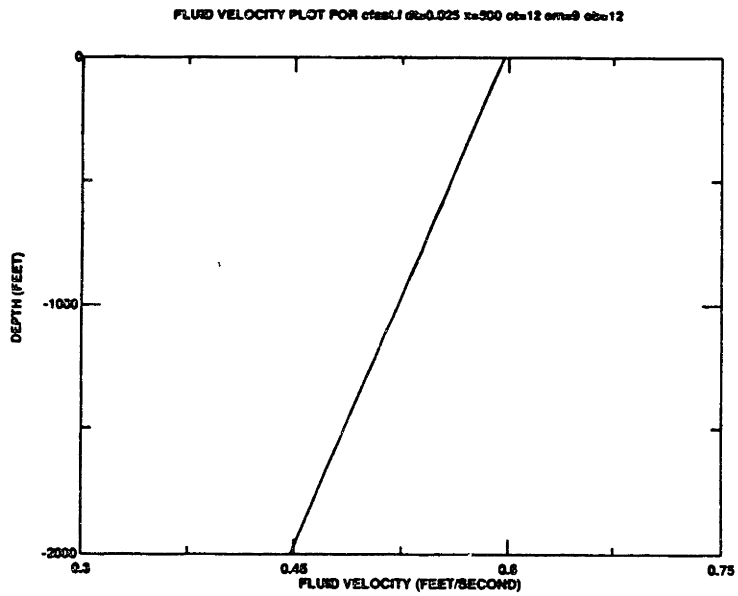

Figure 4-5: Fluid velocity profile for case #1

The dispersion relation given by equation 3.5b suggests that the generated displacement waves are dispersive in nature. This finding is supported by the numerical

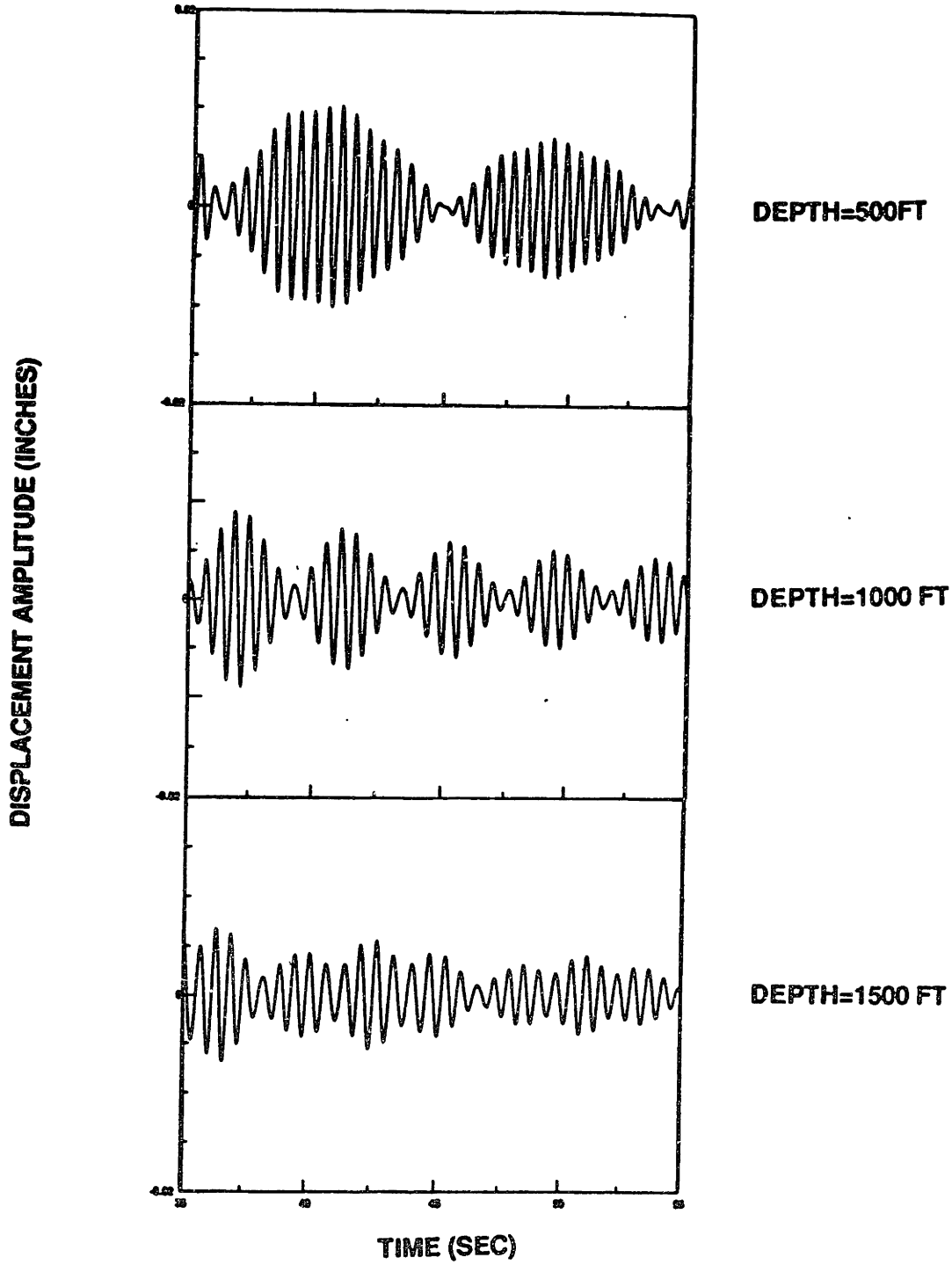

Figure 4-6: Time series records for case #1 excitation profile.

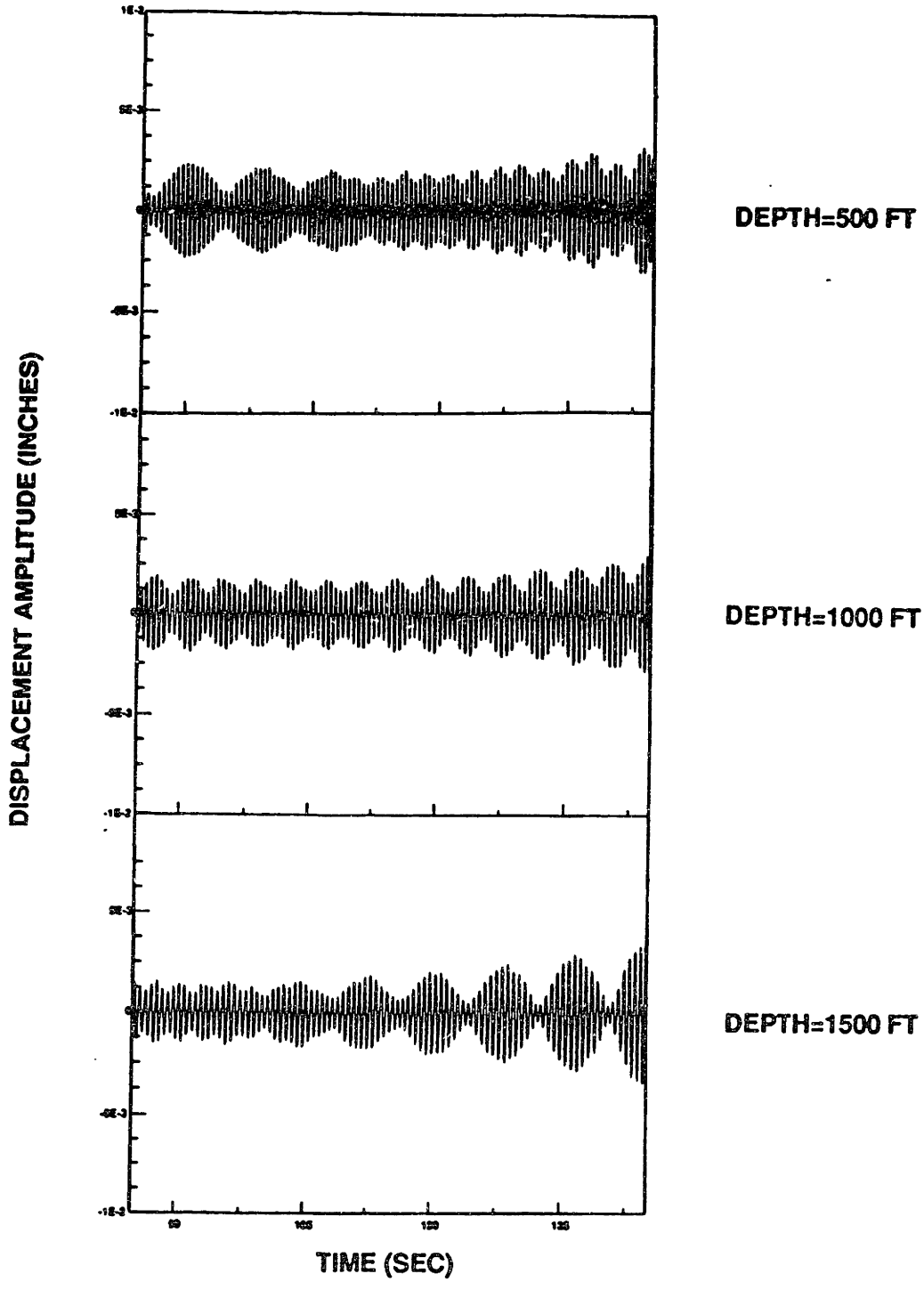

Figure 4-7: Longer time series records for case #1 current profile

results. The clearly defined beats at the 500 ft position shown in figure 4-6 begin to degenerate with time while beating begins to develop at the 1500 foot position. This behavior is demonstrated in the longer time series records shown in figure 4-7. The beat frequency for the 1500 ft position tends to close in on a value that can be determined using the local and low end excitation frequencies. The dispersive nature of the waveforms also serves to effect the amplitude of the overall displacement envelope. That is, the amplitude of the beats is in general nonuniform as demonstrated in figure 4-6.

The effect of a symmetric velocity profile, as shown in figure 4-8, was also studied. Again, no phase angles were used to uncorrelate the excitation. The obtained results were very similar to those described previously as beating occurred which degenerated with time. As predicted, the results were symmetric about the cable midpoint and two time series records are shown in figure 4-9. These records correspond to the quarter chord and midpoint of the cable. The calculated beat frequencies, based on the exciting frequencies at the point of interest and the top of the cable correspond very well with those shown in the time series records.

The fluid velocity profile shown in 4-10 was used to investigate the interaction between two different excitation cases. The results showed that, for the most part, the interaction effects were minimal as the top half of the cable exhibited virtually no amplitude modulation with time. On the contrary, the lower cable section behaved in much the same fashion as in the previously discussed cases. Time series records for the quarter and three-quarter chord positions are presented in figure 4-11. The beat frequencies shown can be predicted using the excitation frequencies discused earlier. Degeneration of the beats did not occur as rapidly in this case. This is due to the fact that the displacement waves generated over the top end of the cable are nondispersive.

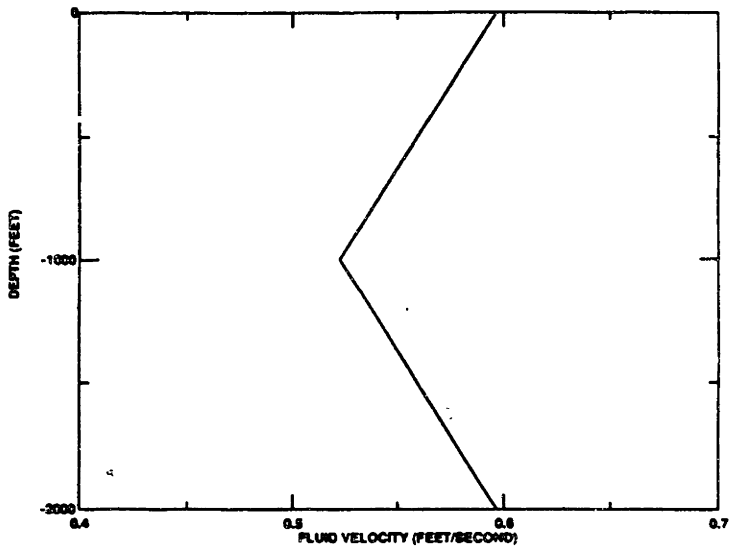

Figure 4-8: Fluid velocity profile for case #2

As mentioned earlier, excitation forces are generally not well correlated along the length of the cable. The SCVP model provides an opportunity for studying the effects of altering the correlation length. This is accomplished by shifting the phase of the excitation forces along the the length of the cable. The linearly varying velocity profile in figure 4-5 was used to analyze the vibration characteristics of the cable midpoint for correlation lengths of 20, 100, and 2000 ft. The last case corresponds to complete correlation of the excitation forces and is used for comparison purposes. The three resulting time series records are presented in figure 4-12. As readily seen, the beating still occurs. However, the beat frequency is no longer well defined. This is due to the large degree of randomness introduced into the problem. The magnitude of the resulting motions also seemed to be affected by the degree of correlation, with larger displacements occurring, in general, for decreased correlation lengths.

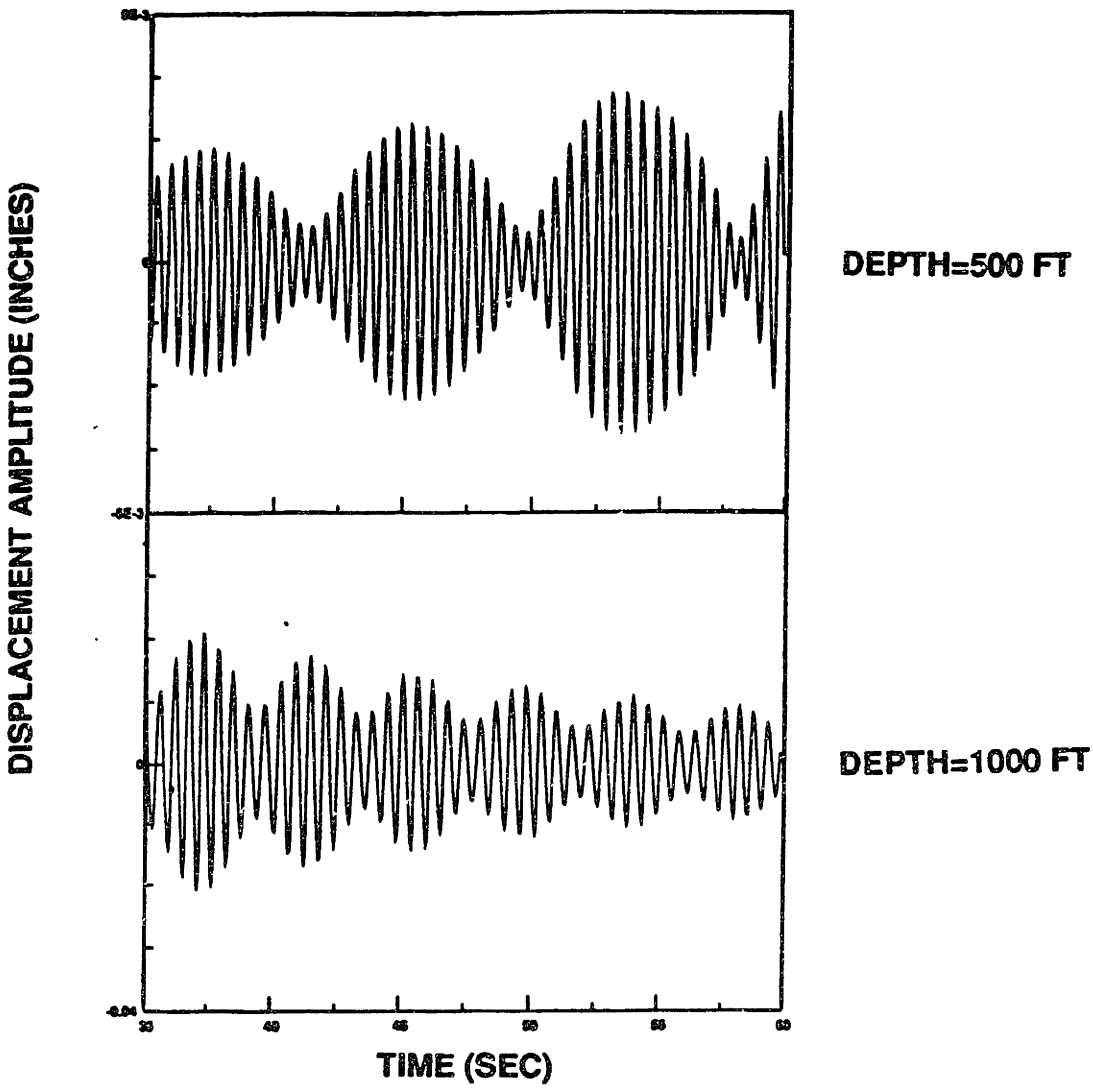

Figure 4-9: Time series records for case #2 excitation profile

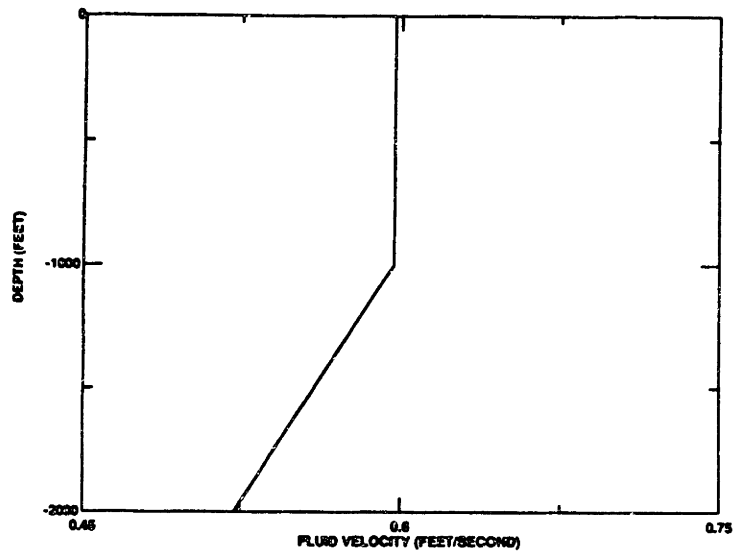

Figure 4-10: Fluid velocity profile for case #3

The actual physical process being modeled does not exhibit the degree of order simulated in the SCVP model. In order to introduce some additional randomness, the method was modified such that initially discrete points are chosen as before but in addition a region is constructed bracketing each point. A point is then selected, at random, within each region and the excitation magnitude and frequency calculated. The determined values are then applied at the original discrete point in the region. Therefore, in the limit as the bracket length goes to zero, the results will converge to those previously obtained. An analysis was completed using the case #1 current profile with total correlation of the excitation forces. Once again, the motions of the cable midpoint were studied. Results for various bracket region sizes are shown in figure 4-13. A 100% bracket region corresponds to a region, centered on the discrete point, of length equal to the spacing between points,

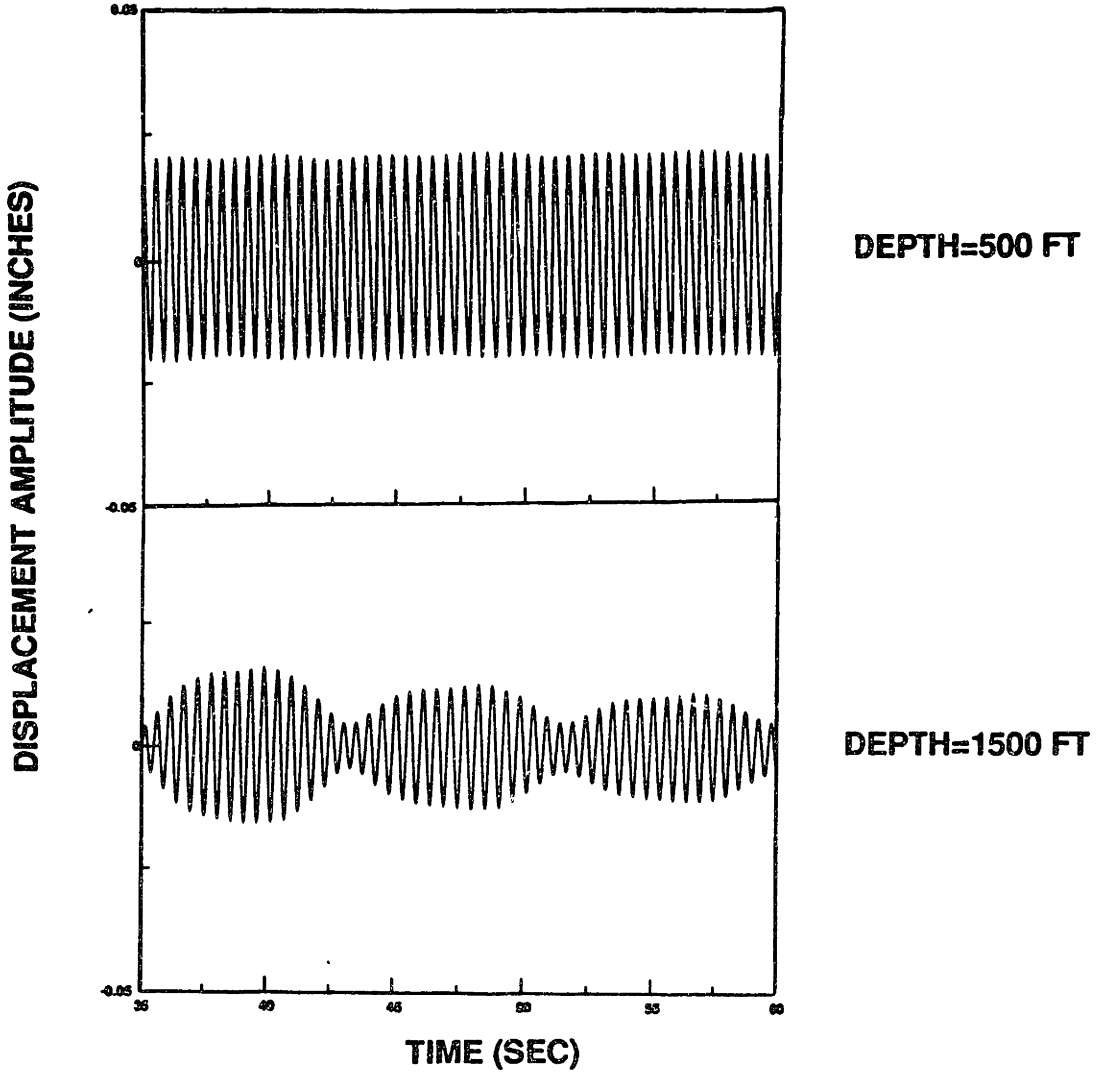

Figure 4-11: Time series records for case #3 excitation profile

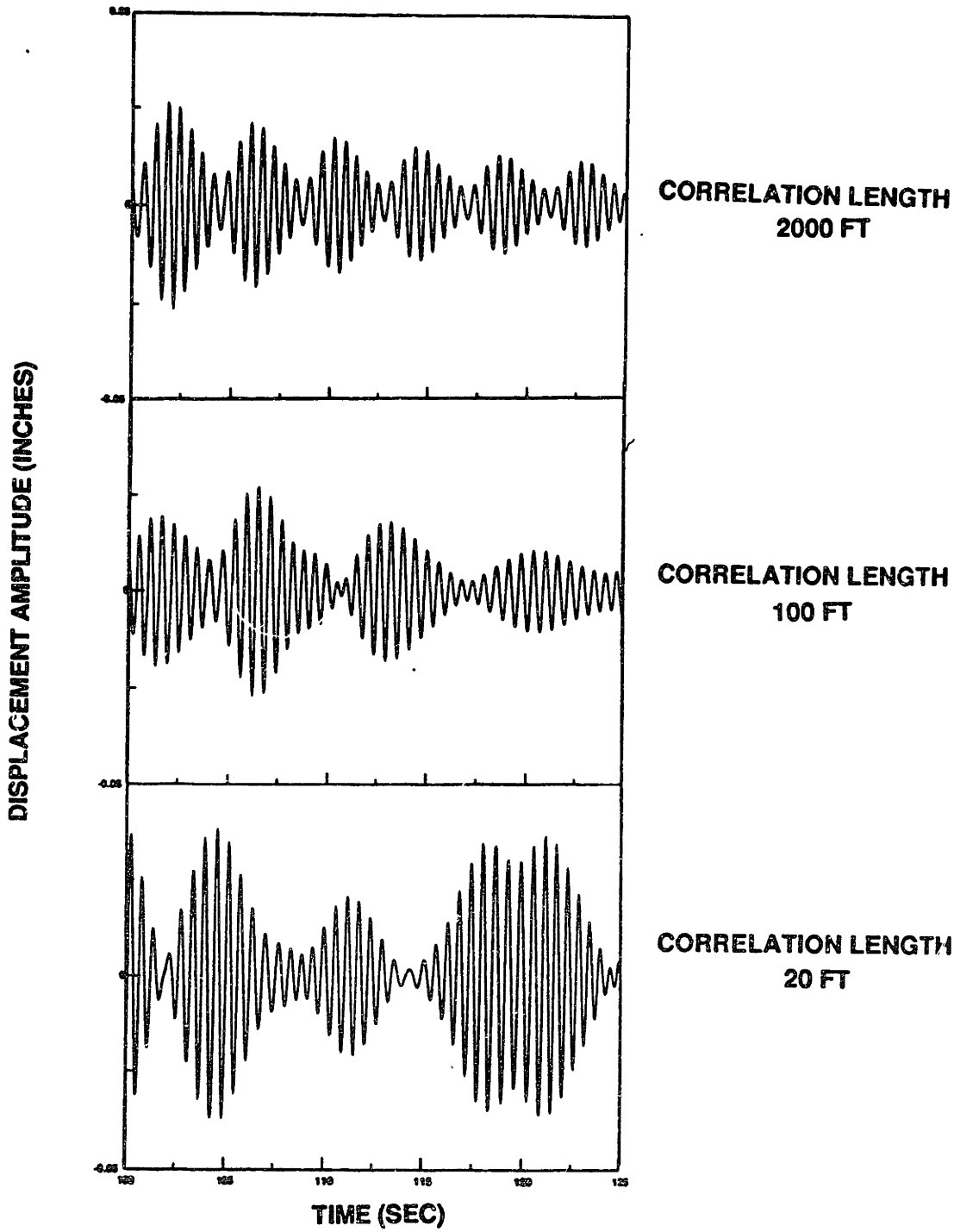

Figure 4-12: Effect of decreased correlation length on vibrations of cable midpoint excited by case #1 current profile

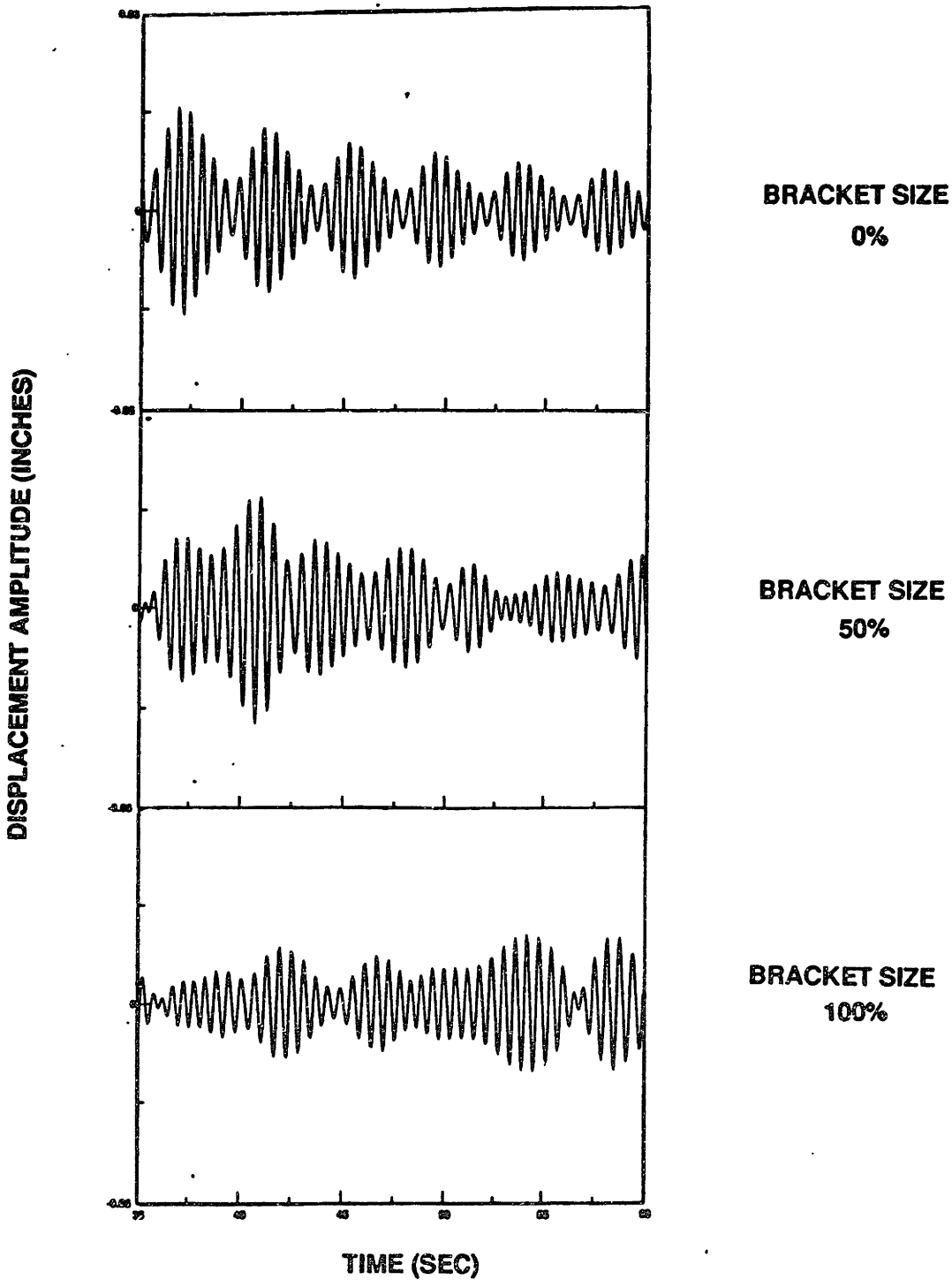

Figure 4-13: Comparison of various bracket regions for randomized excitation forces.

while a 0% value equates to using the originally selected discrete points. As readily seen, an irregular form of beating results which is more prevalent for the increased bracket sizes.

The effect of damping was analyzed by testing a range of values for the damping coefficient β. Damping was determined to have profound impact on the vibration characteristics of the cable. Increased damping resulted in decreased amplitude modulation of the time series. This feature is demonstrated by the time series records presented in figure 4-14. These records correspond to the vibration of the cable midpoint when the cable is excited by the current profile in figure 4-5. As the damping is increased, significant attenuation of the displacement waveforms occurs. As a result, the interaction between displacement waves of different frequencies is reduced, thereby decreasing the amplitude modulation in the time series. These findings are encouraging in that previous research tends to suggest that significant attenuation does occur while the SCVP model appears to be modeling the process correctly, allowing one to study the effects of attentuation in a simple way. The numerical procedure was determined to be stable when damping was eliminated and the resulting time record was very similar to the case with β=0.1.

As mentioned in Chapter 3, there was some desire to construct a model which employs a variable lift coefficient, based on the amplitude of the cable displacement, in order to account for the self-limiting nature of these vibrations. The model shown in figure 3-2 was implemented along with a procedure for determining an envelope which encloses the cable shape at preselected intervals. A typical example of a constructed envelope is shown in figure 4-15. The net effect was a smoothing of the time series as larger motions were reduced while smaller motions went relatively uneffected. These results are easily visualized and as such no time series records will be presented depicting these findings.

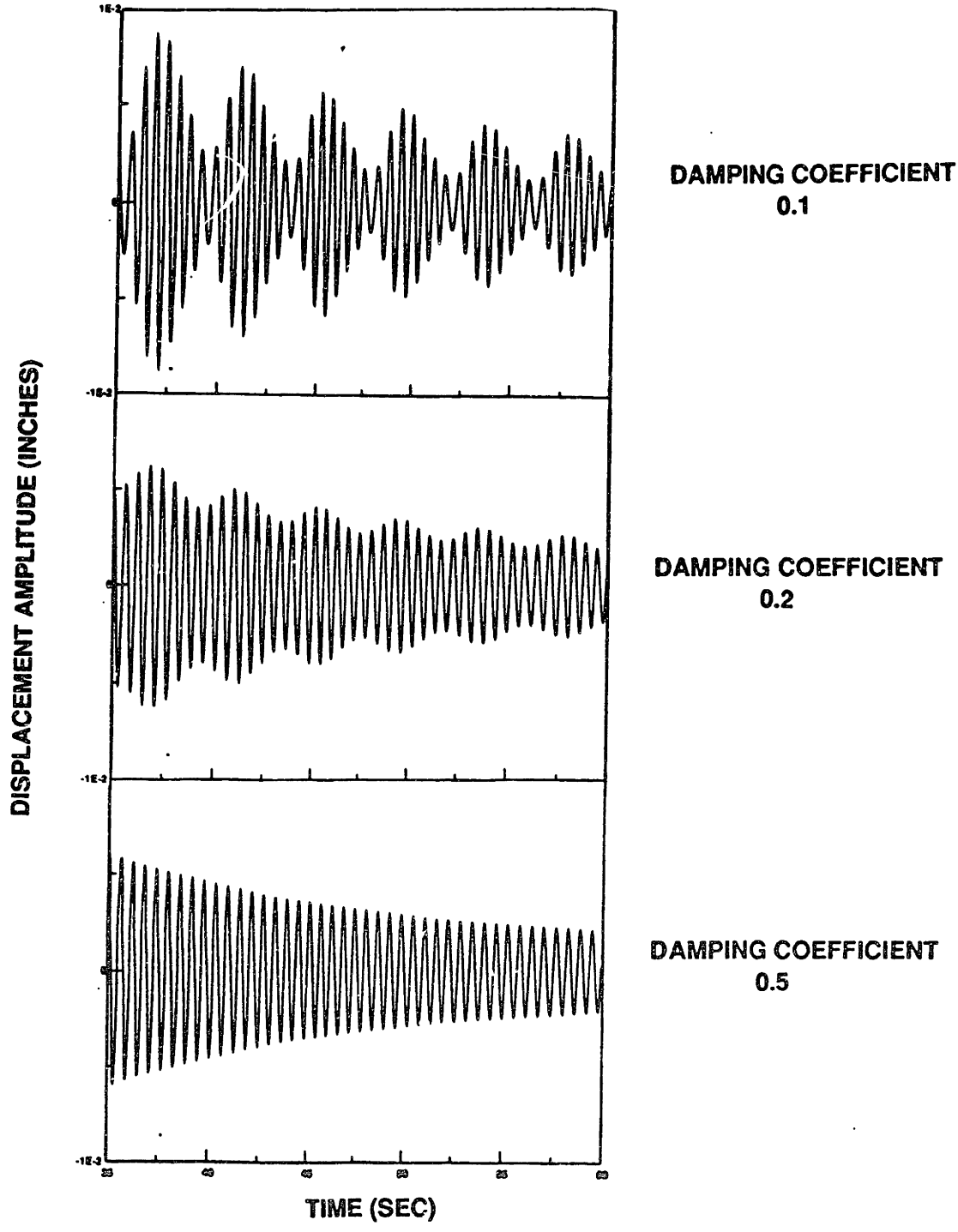

Figure 4-14: Comparison of results for various damping coefficients.

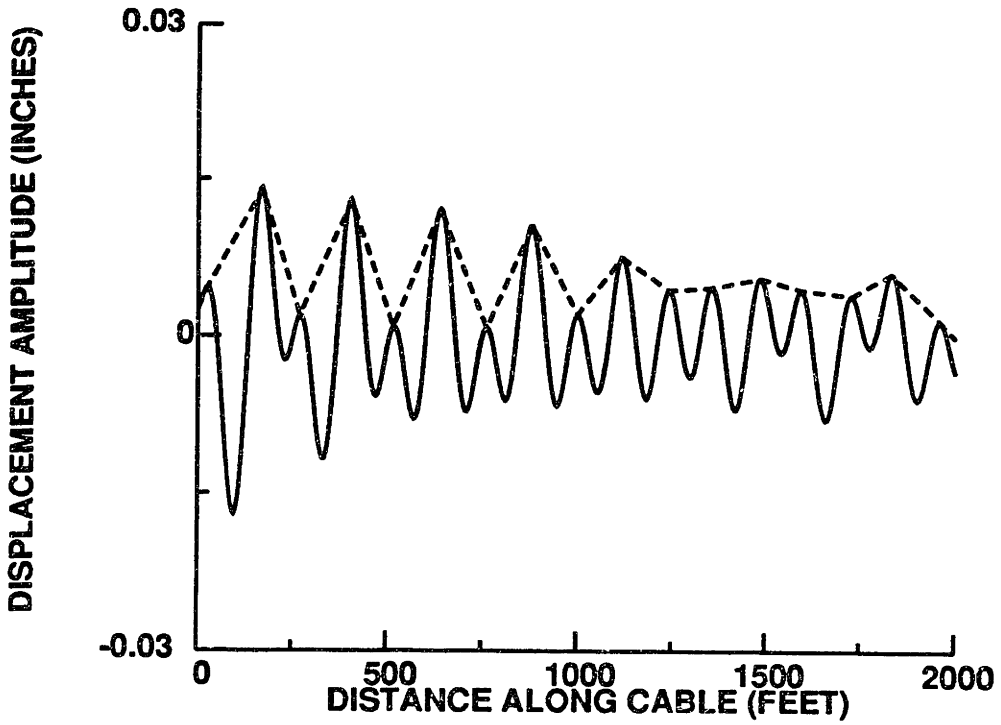

Figure 4-15: Cable shape and associated displacement envelope used for variable lift coefficient model

Chapter 5

Spectral Analysis of Full-Scale Experimental Data

An analysis of full-scale experimental data was conducted in order to validate the findings of the analytic studies. In the experiment, a long cable and spherical ball arrangement was towed and the acceleration measured at discrete points along the cable. A spectral analysis was performed to determine the vibration frequencies and the determined values correlated with the known current profile. Pre-processing of the data proved useful and the methods employed are discussed in this chapter.

5.1 Discussion of Experiment

The data analyzed in this research was obtained in a 1987 experiment conducted at the U.S. Navy's Atlantic Undersea Test and Evaluation Center (AUTEC). A detailed discussion of the experimental apparatus and procedure is presented by Engebretsen [2]. Therefore, only the salient points will be mentioned at this time. The specific data investigated corresponds to the steady-state portion of the fourth experimental run, in which a 2200 kg sphere was attached to the end of a 1220 m cable. The characteristics of the cable are given in table 5-I.

The cable and vehicle were monitored with six acoustic pingers, one fixed to the ship's bottom and others spread along the cable. An array of hydrophones fixed to the sea floor received the acoustic signals. Five instrument packages were also placed on the cable, in-between the acoustic pingers. These packages were used to measure the local cable attitude and acceleration. Triaxial accelerometers were used so that both transverse and

Diameter	0.0173 m
Mass per Unit Length (Air)	1.04 kg/m
Mass per Unit Length (Water)	0.77 kg/m
Young's Modulus	4.75×10^{10} N/M^2

Table 5-I: Characteristics of cable used in the experiment

in-line motions could be recorded. Figure 5-1 provides an overview of the typical experimental setup used.

Within the fourth experimental run, the ship was maintained at a constant speed of 0.51 m/sec for 32 min. During this time, a continuous 10 min record of the high frequency cable accelerations was obtained. A sampling rate of 100 hz was used, yielding 60,000 data points. The high sampling rate was used to avoid problems with aliasing from higher harmonics of the cable strumming.

The current profile was measured with bounce pingers and an electromagnetic probe seven times during the course of the experiment. The dominant current direction was at an angle to the ships track, as shown in figure 5-2. The long straight track corresponds to steady-state conditions during which the data was obtained. A typical current profile for the fourth run is shown in figure 5-3. Note that some shear exists in the profile.

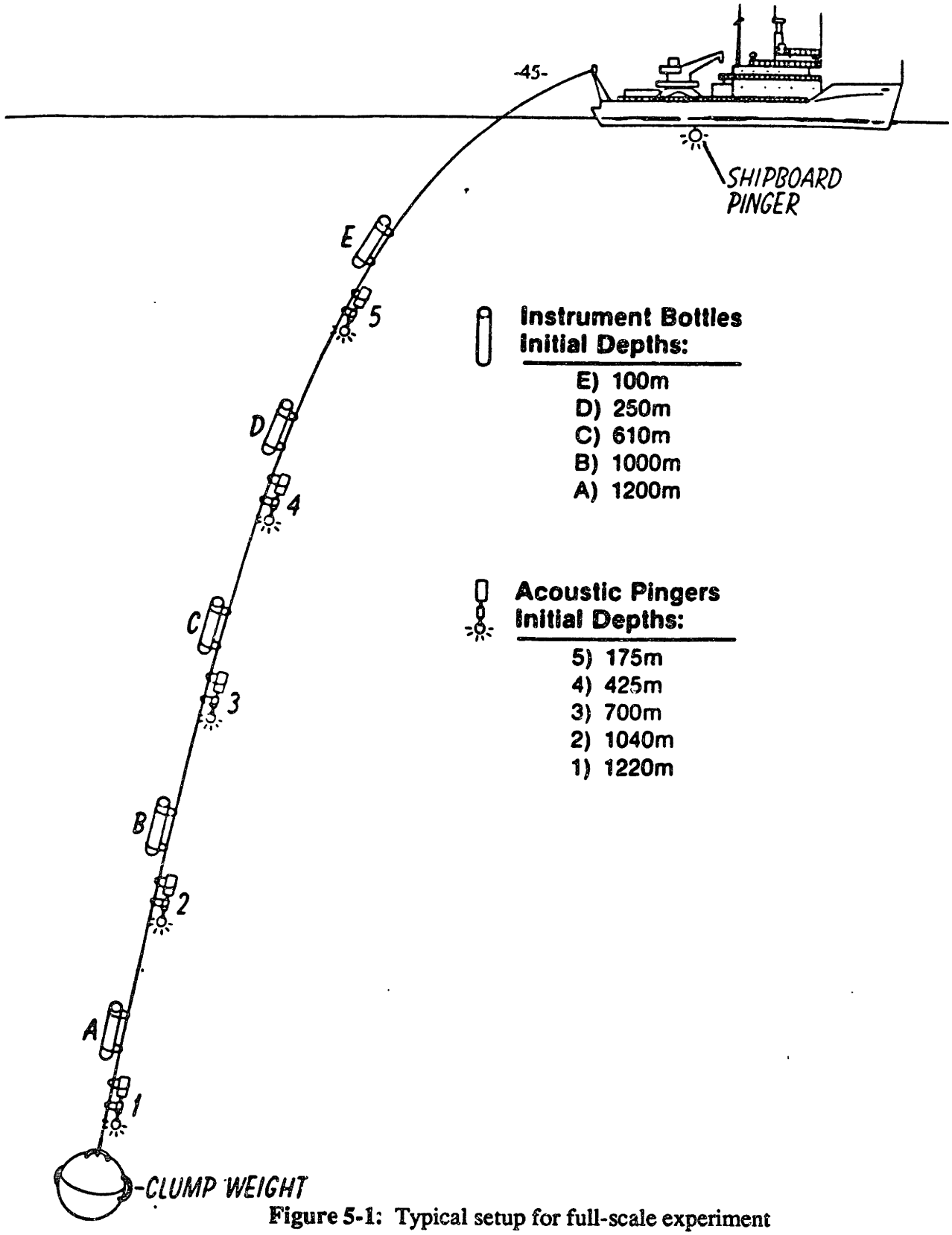

Figure 5-1: Typical setup for full-scale experiment

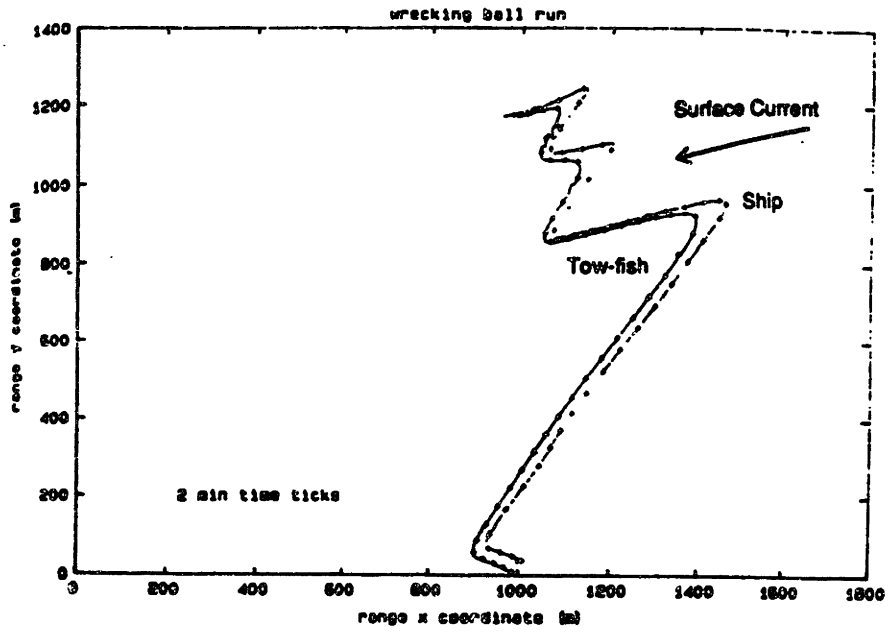

Figure 5-2: Ship course track and current direction for run #4

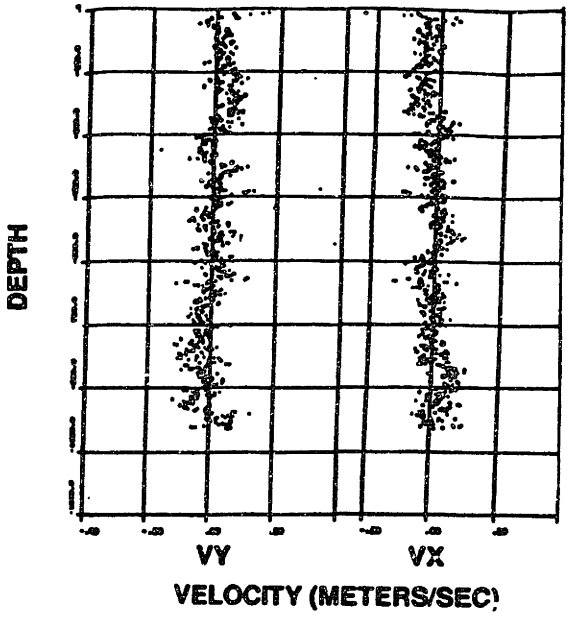

Figure 5-3: Typical current profile for test run #4

5.2 Data Analysis Procedure

5.2.1 Characteristics of Raw Data

Prior to the spectral analysis of the acceleration time series data, the form of the data was investigated to identify possible problem areas. The shear current profile which was prevalent during the sea trails suggests that the time series records should exhibit some form of amplitude modulation. This modulation can be represented as the product of two cosine functions, as shown below.

$$a(t) \sim \cos(\omega_s t)\cos(\omega_b t) \tag{5.1}$$

where

ω_s = strumming frequency

ω_b = beating frequency

$a(t)$ = cable acceleration

Equation 5.1 can be rewritten as the superposition of two cosine functions.

$$a(t) \sim \cos(\omega_1 t) + \cos(\omega_2 t) \tag{5.2}$$

where

$\omega_1 = \omega_s - \omega_b$

$\omega_2 = \omega_s + \omega_b$

The goal of the spectral analysis was to identify the two vibration frequencies so that they could later be correlated with the known velocity gradient. Characteristically, the beat frequency is much less than the strumming frequency. Therefore, the two frequencies given by equation 5.2 will be very close in magnitude. This creates difficulties with the spectral analysis as the two peaks in the spectrum will lay very close together, appearing as

one peak if ω_b is small enough. If the data is not processed in some fashion, extremely high resolution of the spectrum is required. For a time record of predetermined length, this means increased variance in the results and, in turn, decreased accuracy. Therefore, the data must be processed in some form to facilitate the identification of the frequencies. Two methods were chosen for accomplishing this task, namely homomorphic processing and the so-called envelope approach. These methods are described in the following sections.

5.2.2 Homomorphic Processing

The term homomorphic systems is used to describe nonlinear systems that obey a generalized principle of superposition [6]. The goal of homomorphic processing is to exploit this characteristic so as to create an associated linear system that can be analyzed with greater ease. The cable acceleration signal, as written in equation 5.1, is given by the product of two component signals and, therefore, obeys a principle of superposition for multiplication.

Oppenheim, et al [6], present in detail a technique for analyzing multiplicative homomorphic systems. The method is based on determining a function that will transform a multiplicative input signal into a signal comprised of the summation of two component signals. The function which has this property is the logarithm function. By performing the logarithm operation the two frequency components may be separated as shown below.

$$\begin{aligned} \log[a(t)] &= \log[\cos(\omega_b t)\cos(\omega_s t)] \\ &= \log|\cos(\omega_b t)| + \log|\cos(\omega_s t)| \\ &+ i\,arg\{\log[\cos(\omega_b t)]\} + i\,arg\{\log[\cos(\omega_s t)]\} \end{aligned} \tag{5.3}$$

The fact that the acceleration signal takes on negative values necessitates the use of the complex logarithm. This creates some ambiguity as the imaginary part of the complex

logarithm is not uniquely defined. Any integer multiple of 2π can be added to the imaginary part without changing the results. This problem cannot be resolved by replacing $arg\,[a(t)]$ by its principle value as it is not generally true that the principle value of the sum of two angles is equal to the sum of their principle values. To resolve this ambiguity, equation 5.4 must hold and $arg\,[a(t)]$ must be defined such that it is a continuous function of $a(t)$.

$$arg\,[a(t)] = arg\{\log[\cos(\omega_b t)]\} + arg\{\log[\cos(\omega_s t)]\} \qquad (5.4)$$

Once the imaginary part of the signal has been uniquely defined, the signal may be treated as a simple linear system and operated on as such. After the linear operations, such as filtering, are performed, the complex exponential function can be used to transform the signal to its multiplicative form. The canonic representation for this processing is shown in figure 5-4.

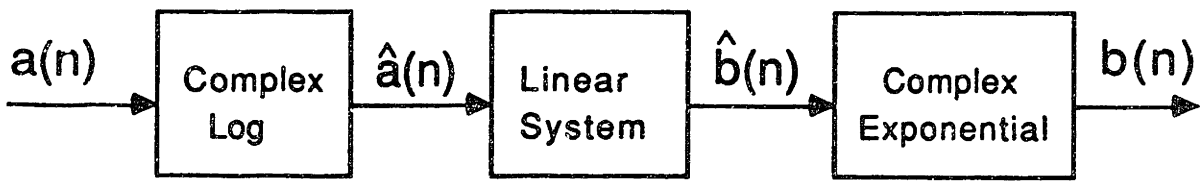

Figure 5-4: Canonic representation of homomorphic system

For the purposes of this investigation, the spectrum for the real part of the processed

signal is sufficient for identifying the frequencies of interest. This alleviates the problems associated with the imaginary part as described above. It should be noted that the frequencies in the real spectrum will lay at twice the defined frequencies because the absolute value of the signal is used in the logarithm, causing the vibration frequencies to double. In addition some higher order harmonics are excited because the signal is no longer sinusoidal in shape.

5.2.3 Envelope Approach

The second method employed for simplifying the identification of the vibration frequencies is called the envelope approach. This method is based on elimination of the high frequency motions of the cable so as to identify the beating frequency. This is accomplished by constructing an envelope which completely encloses the acceleration time series. The envelope is determined by locating all positive peaks in the time series and then assuming a linear variation between these peaks. A spectral analysis is then performed on the envelope signal. This method has its mathematical basis in that the envelope of the amplitude modulated signal is close to sinusoidal. The frequency associted with the envelope is twice the defined beat frequency as each oscillation corresponds to one beat in the time series.

5.2.4 Power Spectrum Calculation

The central item in analyzing the full-scale experimental data is the estimation of the acceleration power spectra. The power spectrum relates the power in the signal to its associated frequency bands. Therefore, the dominant vibration frequencies may be determined by identifying the frequencies at which peaks in power occur. A wide variety of methods exist for power spectrum estimation and the one chosen for this analysis is called the Welch method.

The statistical quantity know as the periodogram may be used as an estimate of the spectrum. The periodogram, denoted by $I_N(\omega)$, is determined from the Fourier transform of a real sequence $x(n)$, containing N samples, as shown below.

$$I_N(\omega) = \frac{1}{N}|X(e^{i\omega})|^2 \tag{5.5}$$

where $X(e^{i\omega})$ represents the Fourier transform of $x(n)$ and can be determined as follows:

$$X(e^{i\omega}) = \sum_{n=0}^{N-1} x(n)e^{-i\omega N} \tag{5.6}$$

Unfortunately, the variance of $I_N(\omega)$ does not approach zero as N approaches infinity. Therefore the periodogram is not a consistent estimate of the spectrum. It can be shown that the variance of the average of K independent periodograms is a consistent as the variance is a function of $1/K$ [10]. This would suggest that for a record of fixed length $N=KM$, it would be advantageous to choose K as large as possible. However, as K increases M decreases, subsequently reducing the resolution of the spectrum. Thus there is a tradeoff between spectrum resolution (bias) and variance.

To further help reduce the spectral variance, overlapping of segments may be performed. In this method, the length of the time record is effectively increased by constructing additional segments which overlap existing segments. It turns out to be optimal to overlap segments by one half their length [7]. This increases the total number of available segments to K', where $K'=2K-1$. The reduction in the variance is not a full factor of K' since the segments are not statistically independent. Rather, the variance is reduced by a factor of about $9K'/11$ [7].

As mentioned earlier, the cost of choosing more segments within the time series is

reduction in the spectral resolution, also termed increased bias. The true power spectrum is based on a time series of infinite length. Using a finite length series causes energy leakage into other frequencies. This effect is amplified with decreased record lengths. To overcome this, smoothing of the periodogram by convolution with an appropriate spectral window may be used. A wide variety of spectral windows are available for this purpose [7]. Several windows were implemented in this analysis and the window which best suited the data is presented in each case.

The Welch method is basically a composite of the techniques discussed above. It consists of the averaging of modified periodograms. The data is sectioned into K segments, or K' if overlapping is employed, of length M. The window $w(n)$ is applied directly to the data segments before computation of the periodogram. This yields K periodograms

$$J_M^{(j)}(\frac{2\pi K}{M}) = \frac{1}{MU} | \sum_{n=0}^{M-1} x^{(j)}(n)\, w(n)\, e^{-i(2\pi/M)Kn} |^2 \qquad (5.7)$$

where

$$U = \frac{1}{M} \sum_{n=0}^{M-1} [w(n)]^2$$

The power spectrum S_{xx} may then be estimated by averaging the modified periodograms.

$$S_{xx}(\frac{2\pi K}{M}) = \frac{1}{K} \sum_{j=1}^{K} J_M^{(j)}(\frac{2\pi K}{M}) \qquad K = 0,1,....,M-1 \qquad (5.8)$$

The FFT (Fast Fourier Transform) method is used to compute the absolute value term in equation 5.7. The accuracy and ease with which this method may be implemented dictated its use in this research.

5.2.5 Example Analysis

An analysis of the two point excitation results shown in section 4.1 is presented to demonstrate the abilities of the data processing techniques employed. Recall that the exciting frequencies of 8.5π and 9.0π rad/sec gave rise to visually determined beating and strumming frequencies of 0.25π (.785) and 8.75π (27.49) rad/sec, respectively. The power spectrum for the original signal is shown in figure 5-5. The spectrum was generated using 10 original segments of 1200 points. Overlapping was implemented to create 19 dependent segments and a Tukey window was used for spectral smoothing. The power spectrum shows two closely spaced peaks occurring at the frequencies given by equation 5.2. Homomorphic processing was used to separate the peaks and the resulting spectrum is shown in figure 5-6. This figure clearly demonstrates the accuracy of the method as energy peaks were determined at twice the vibration frequencies, as predicted. Specifically, the peaks occur at 1.571 and 54.978 rad/sec. The smaller energy peaks shown are a by-product of the method. Results obtained using the envelope approach are shown in figure 5-7. This figure shows that this method effectively filters the high frequency motions and yields a correct solution for the beat frequency. Having verified the accuracy of the processing techniques with a known problem, we may now proceed to analyzing the full-scale experimental data.

5.3 Presentation of Results

The data analyzed consisted of 9 time series records of 60,000 points, sampled at a rate of 100 hz. These records included the transverse and in-line motions for each of the five instrument bottle locations with the exception of the in-line motions of bottle E. This data was not recorded. All the data was zero-meaned and calibrated prior to processing.

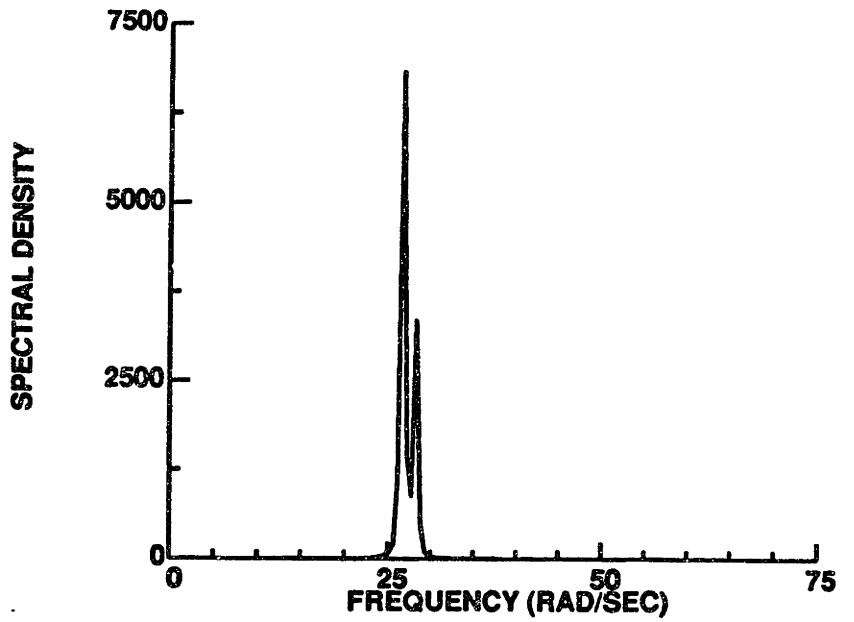

Figure 5-5: Power spectrum for unprocessed signal

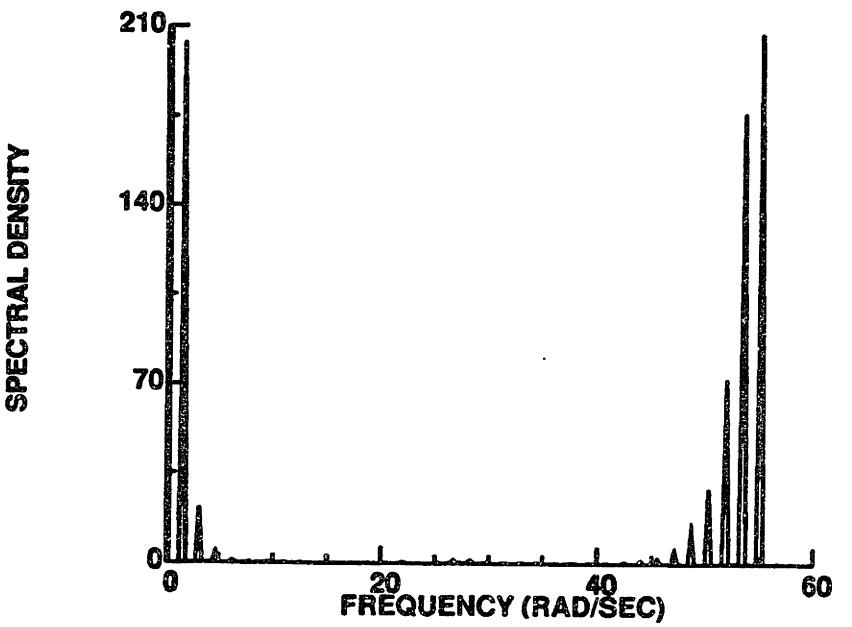

Figure 5-6: Power spectrum after homomorphic processing

The long time series records provided a basis with which accurate spectral estimates could be obtained as requirements for spectral resolution and variance reduction could both be

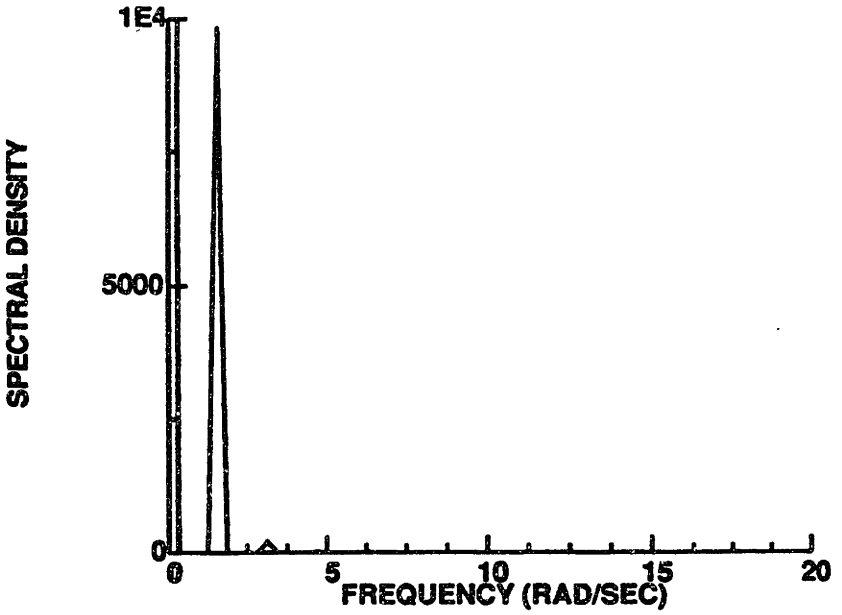

Figure 5-7: Power spectrum for envelope of original signal

met. However, it is possible for the process to become non-stationary over this long period due to changes, for example, in the ship speed. This point will be discused in more detail later in this chapter. The high sampling rate helped to avoid problems with aliasing for higher harmonics of cable strumming.

The first step in the investigation was to verify which data channel on the triaxial accelerometers recorded the transverse cable motions. In the initial configuration, channels 0 and 1 were set to record the transverse and in-line motions, respectively. The reasoning behind this study was to ensure that the instrument bottles did not become twisted with respect to the cable during the experiment. As mentioned in Chapter 2, the frequency of the transverse cable motions will be given by a value at or near the Strouhal frequency. Some variation may arise as a result of beating but the vibration frequency will remain in a relatively small range around this frequency. The frequency of the in-line motions, however, corresponds to twice the Strouhal frequency. Therefore, the individual data

channels may be identified by determining which channel yields a stronger spectral peak at the Strouhal frequency.

The calculated Strouhal frequency for this experiment was around 32 rad/sec. This value is based on a ship speed of 0.51 m/sec and a Strouhal number of 0.175 as determined from previous research [2]. The power spectra were constructed for each data set using a Tukey window for spectral smoothing. The results obtained are presented in figure 5-8 and the top left plot in figures 5-9 through 5-13. Figure 5-8 shows spectra for the four channel 1 data sets. The spectra have been scaled to roughly equal height by the scale factor SF listed. As readily seen, in figure 5-8 very little energy is located near the Strouhal frequency while considerable energy is associated at twice this frequency. The unprocessed spectra for the channel 0 records, however, all exhibit definite peaks in the Strouhal frequency range. Therefore, we can conclude that the instrument bottles remained correctly aligned and that the transverse motions were recorded on channel 0.

The spectral peak was determined from each calculated spectra and the corresponding frequency values are listed in table 5-II. Note that for the spectra corresponding to the in-line motions, the maximum peak between 50 and 80 rad/sec was selected. These peak values will later prove useful in determining the strumming frequencies. The spectra were generated using overlapping of segments and a range segment lengths was used to confirm the accuracy of the results.

As can be seen in figures 5-9 through 5-13, the spectra are fairly narrow banded near the Strouhal frequency and multiple bands exist within this range. These peaks tend to become more prevalent with increased spectrum resolution. The spectral bands that lie above this range correspond to higher-order harmonics and motions of the instrument bottles. The time series records were all band-pass filtered between 20 and 45 rad/sec to

eliminate these peaks. The resulting time series records were visually inspected and beating did exist. However, no clear pattern was evident. As a result the filtered time series records did not aid in determining the beat frequencies and therefore will not be presented.

Homomorphic processing was performed on the filtered time series and the spectra determined are shown in the bottom two plots in figures 5-9 through 5-13. The plot in the lower left covers a longer frequency range so as to show the high-frequency peak associated with cable strumming. From these plots, the largest high-frequency peak was selected and the value is listed as the second value in the homomorphic processing column in table 5-II. This value was selected because it should give some indication of the strumming frequency. The lower right plot focuses in on the low-frequency range to determine the beat frequency. The spectral resolution or space between data points for these lower plots was 0.052 rad/sec. The first value listed in the homomorphic processing column denotes the most pronounced low frequency peak. This value gives some indication of the beat frequency. The appropriate value to choose was not always clear and was sometimes at the discretion of the analyst. The harmonics generated by this type of processing, the possibility of multiple beat frequencies, and the large peak at zero frequency created by the non-zero-meaned process all give rise to this problem. It is not appropriate to always select the highest peak as this has been proven to be incorrect in cases with a known frequency response. The correct peak to choose is the most distinct peak separated from the zero energy peak. Overlapping was not used in conjunction with this type of processing as its inclusion created totally unrealistic results. The reason for this behavior is not yet known.

After completion of the homomorphic processing, an envelope was constructed from the filtered time series records as described in section 5.2.3. The spectra determined from these new time series are shown in the upper right plots in figures 5-9 through 5-13. These

plots focus on the low-frequency range as all high-frequency energy has been eliminated by the processing technique. The highest and most distinct peak was determined in each plot and the result is listed in the last column of table 5-II. The smaller peaks are a by-product of the method and some care must be excercised in determining which peak to select. The spectrum resolution was 0.052 rad/sec and overlapping proved to be helpful in defining the peaks.

The values in table 5-II were analyzed to determine the frequency estimates listed in table 5-III. The strumming frequencies are based primarily on the largest unprocessed peak and on the high frequency peak determined from homomorphic processing. The difference between the two largest peaks in the unprocessed spectra also played some role in the analysis. The most dominant low-frequency peaks determined by the two processing techniques provided the basis for the beat frequency estimates. The accuracy bounds for the estimates are discussed in the next section.

5.4 Discussion of Results

The power spectra determined from the 9 time series records confirm that the transverse cable motions were recorded on channel 0 for all instrument bottle locations. The unprocessed spectra for this channel definitely show vibrations in the Strouhal frequency range. The spectra, although narrow banded in this region, tended to be multiple peaked. This finding can be attributed to several causes. First of all, the occurrence of beating will tend to split the spectrum as discussed earlier. Secondly, during the ten minute time period over which the data was collected, some variation of the inflow velocity most likely occurred as a result of slight variations in ship speed and current magnitude. For example, a 0.05 m/sec change in the ship speed corresponds to a 3.2 rad/sec variation of the

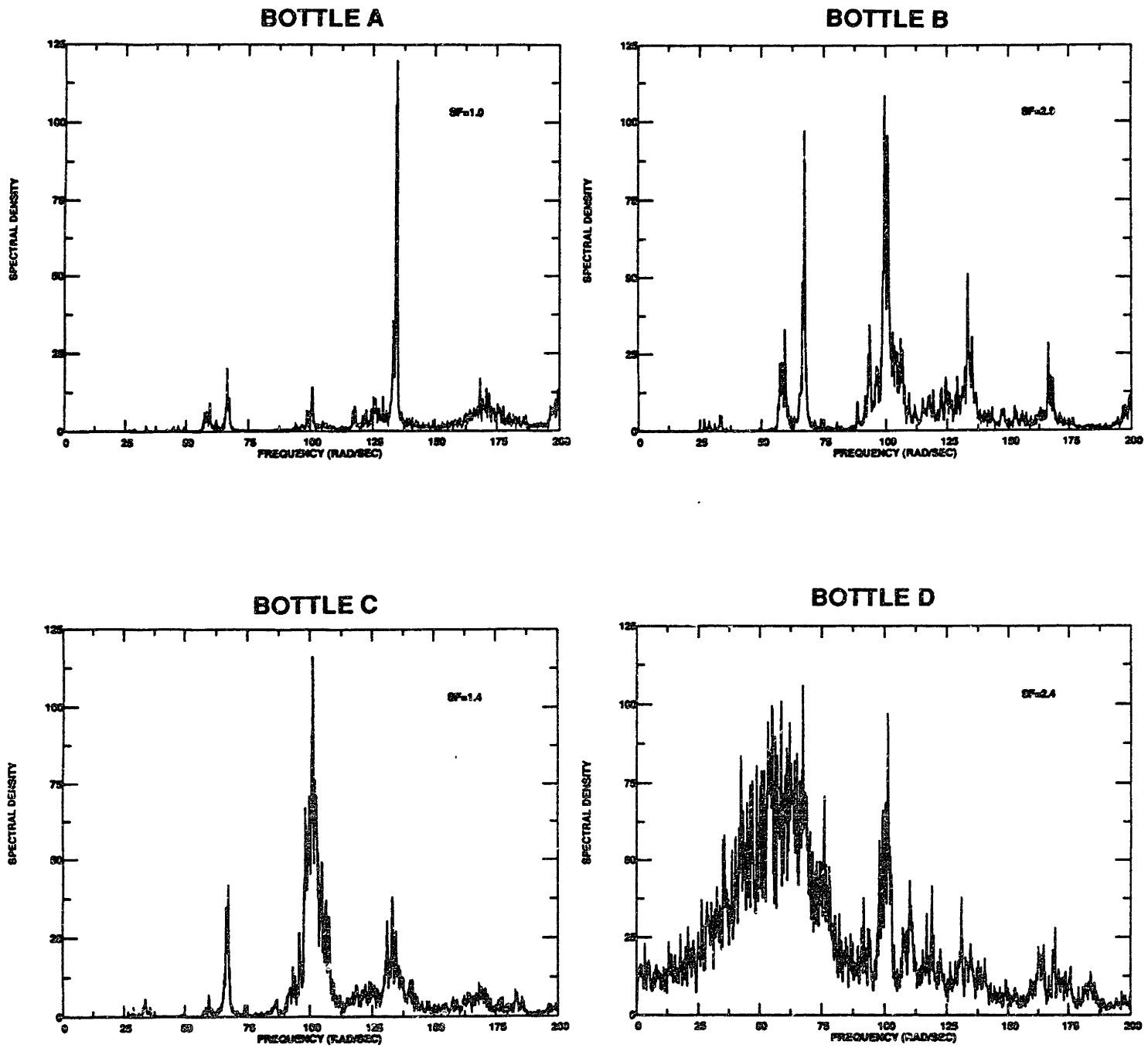

Figure 5-8: Unprocessed power spectra for channel 0 data sets

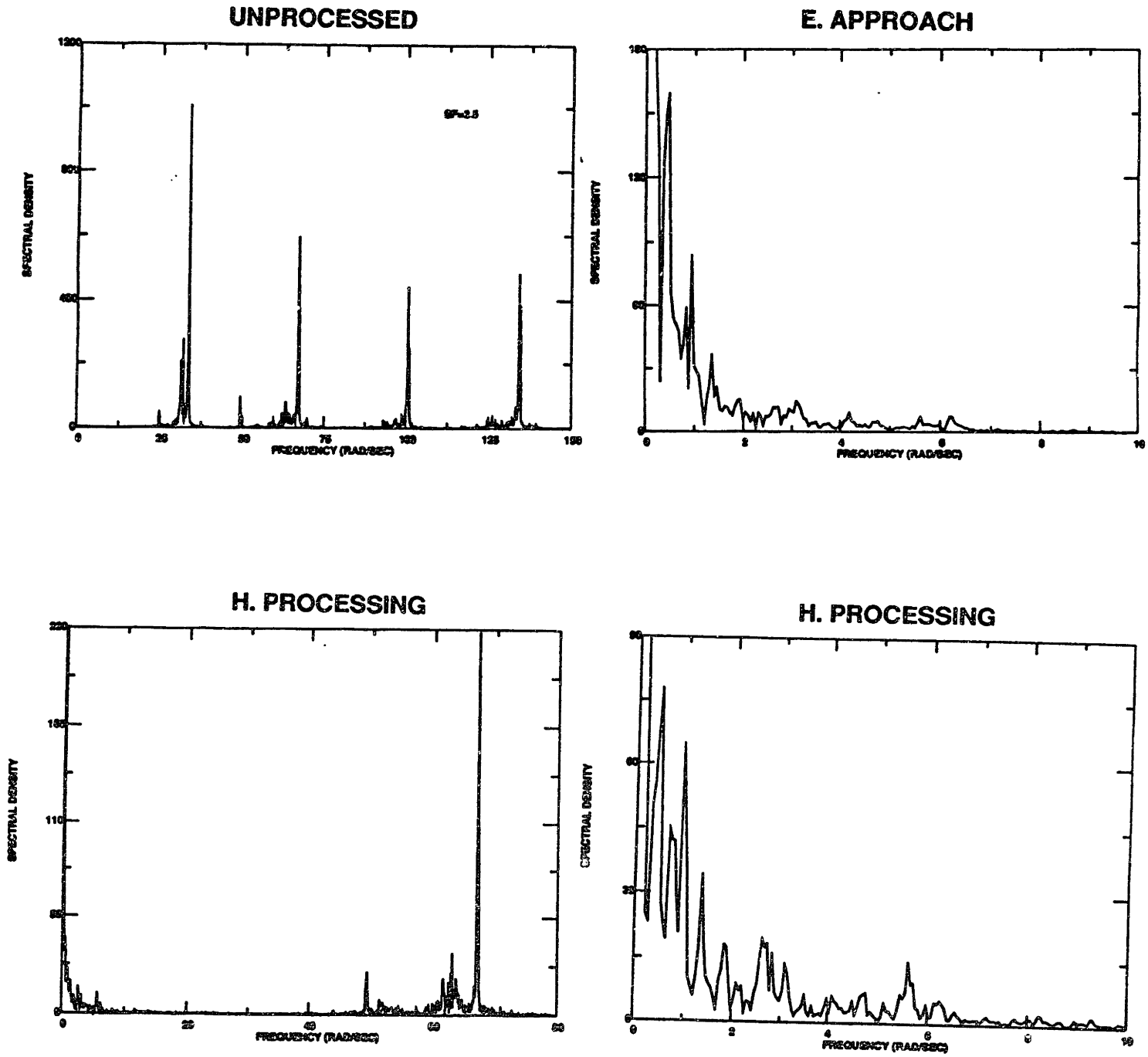

Figure 5-9: Unprocessed and processed power spectra for instrument bottle A

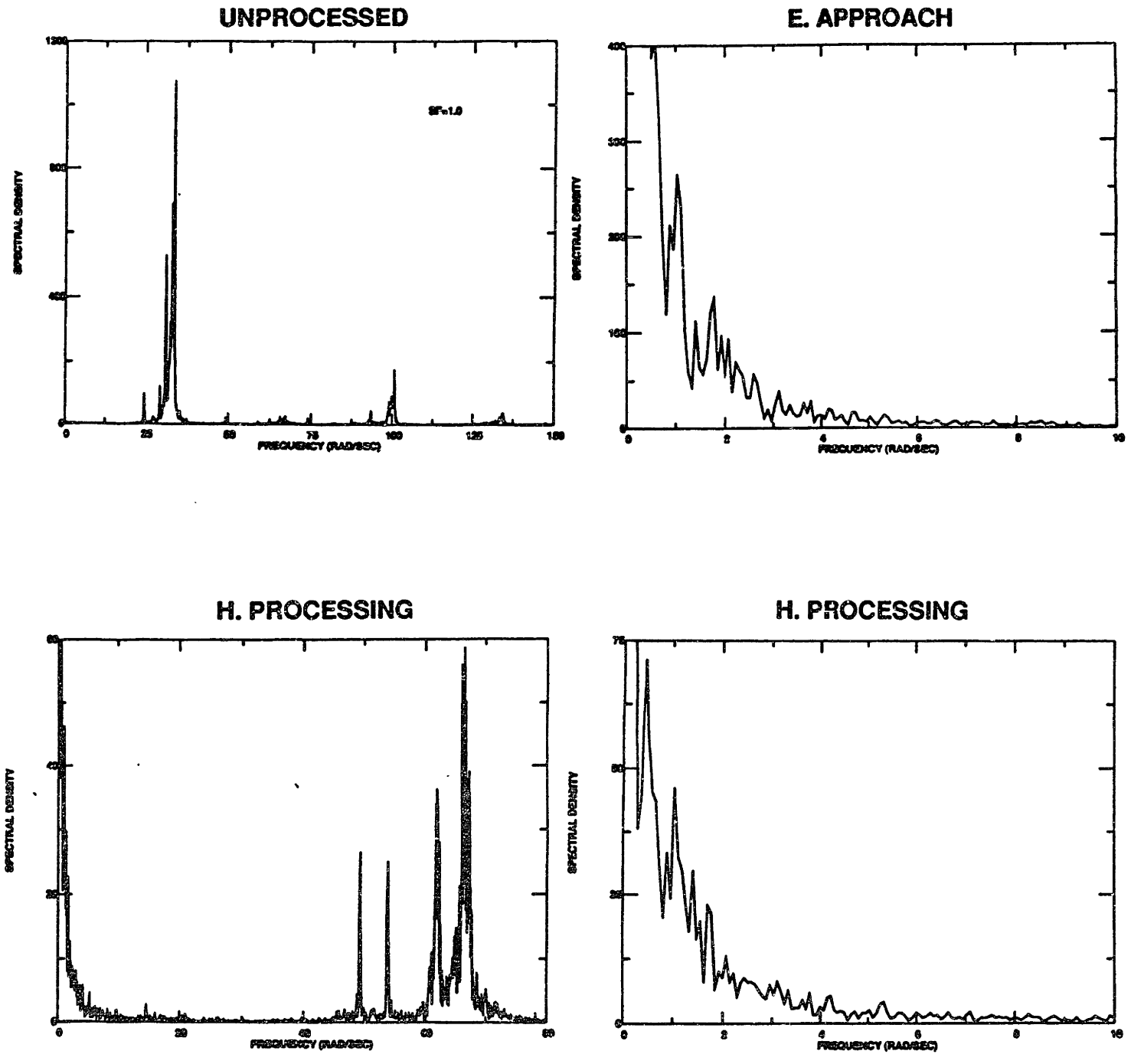

Figure 5-10: Unprocessed and processed power spectra for instrument bottle B

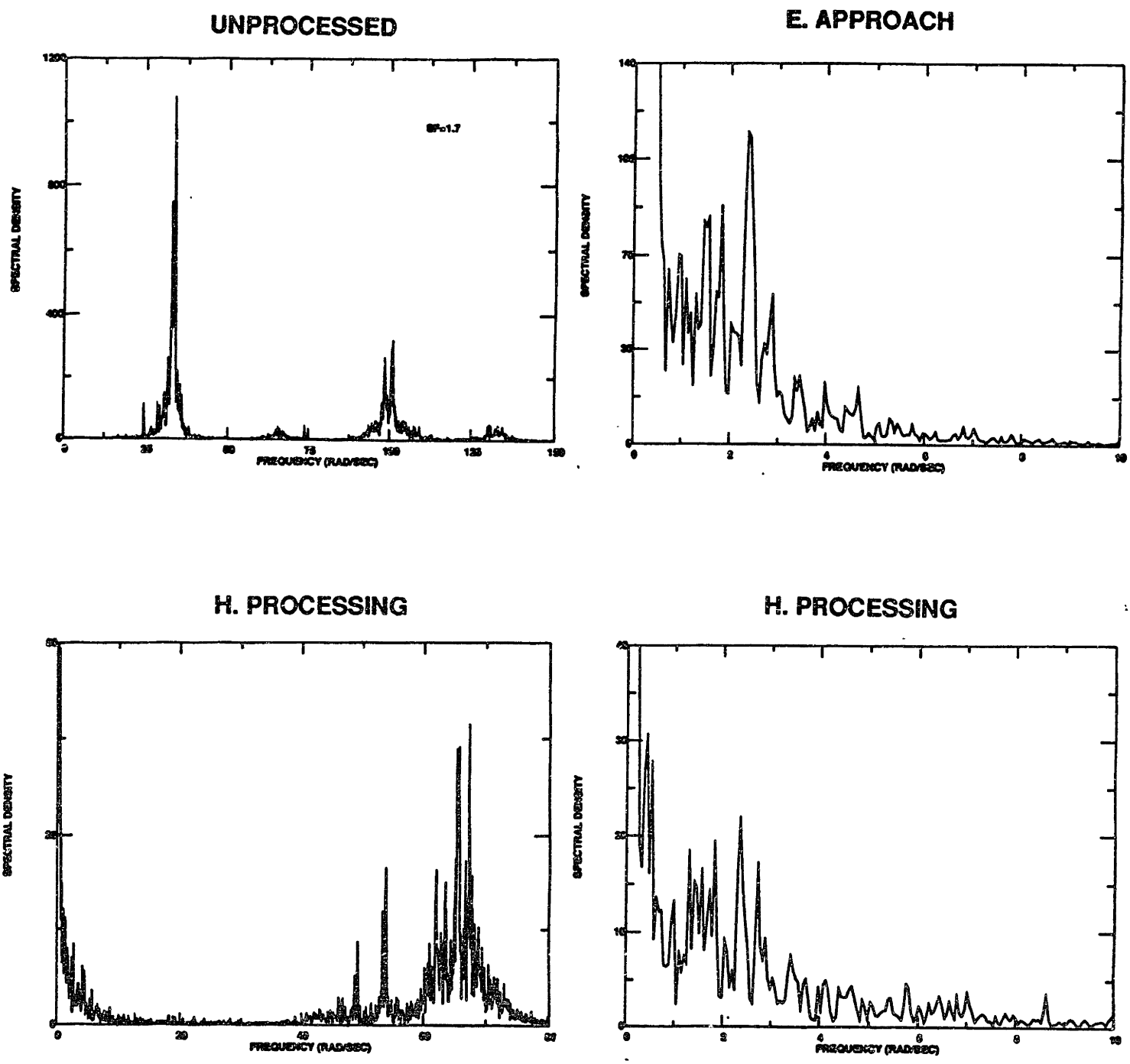

Figure 5-11: Unprocessed and processed power spectra for instrument bottle C

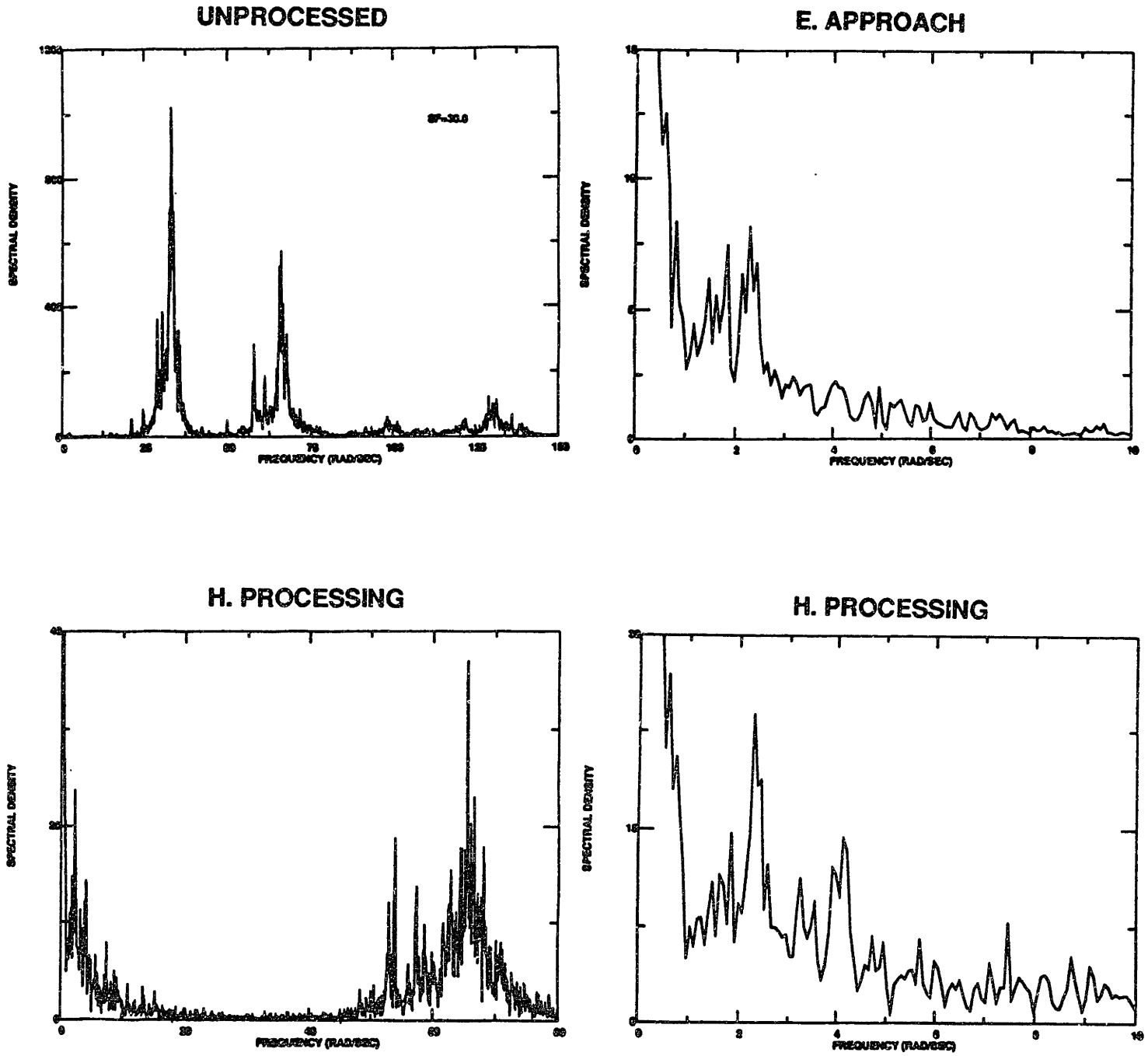

Figure 5-12: Unprocessed and processed power spectra for instrument bottle D

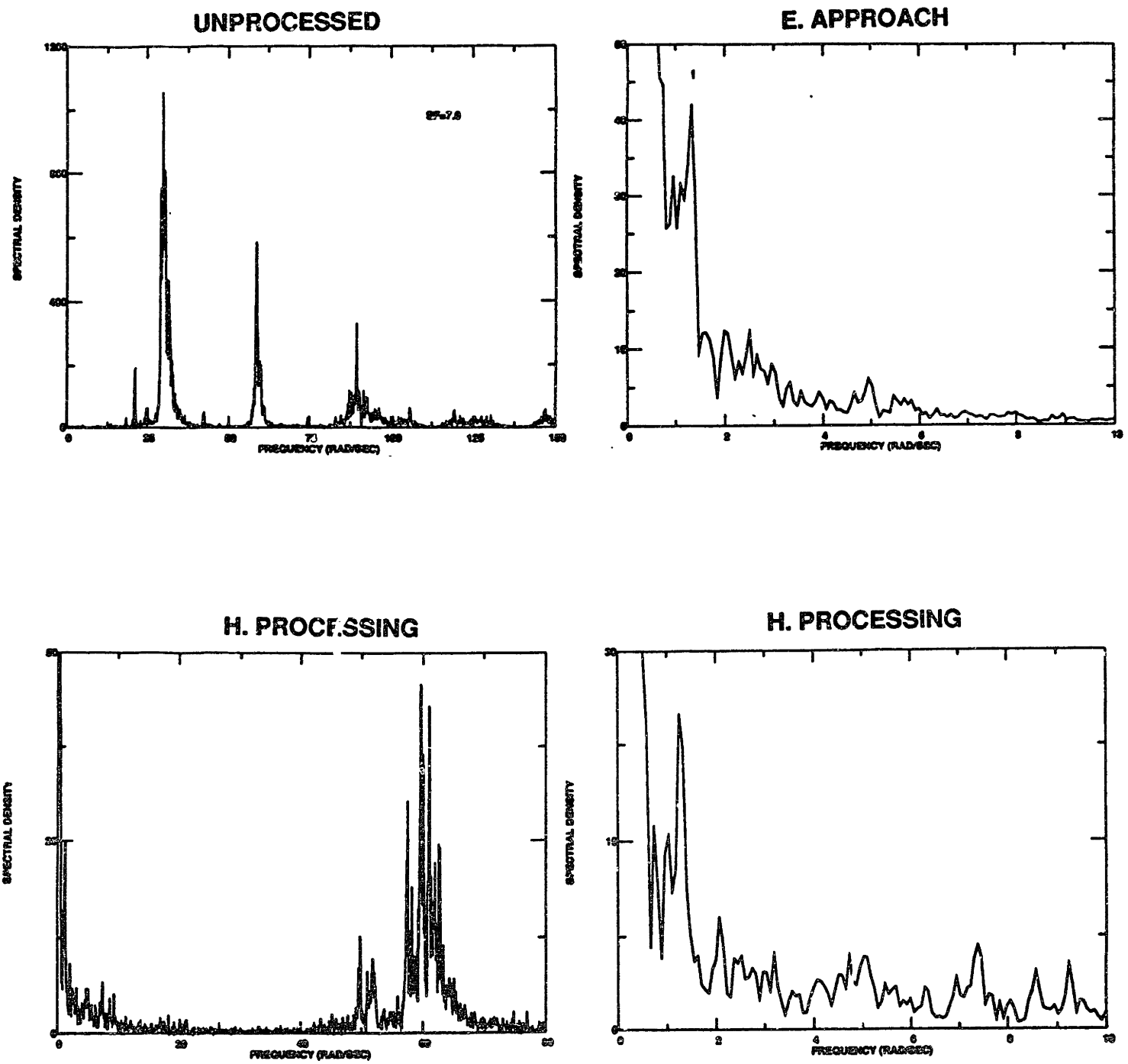

Figure 5-13: Unprocessed and processed power spectra for instrument bottle E

DATASET	SP. PEAK (TRANS.)	SP. PEAK (IN-LINE)	SP. PEAKS (H. PROCESS)	SP. PEAK (E. METHOD)
A	33.5	66.5	0.5/67.1	0.5
B	33.7	67.4	0.5/66.5	1.0
C	33.7	67.4	2.4/67.3	2.4
D	33.3	67.4	2.3/65.6	2.3
E	29.8	——	1.2/59.7	1.3

Table 5-II: Spectral peaks as determined from the spectral analysis

Strouhal frequency. Finally, there are likely to be some dynamic effects caused by the instrument bottles themselves.

Given in table 5-III are the best estimates of the beating and strumming frequencies. The strumming frequencies are all thought to be accurate within 3%, based on variations in the calculated frequencies. Unfortunately a similar comment may not be made about the beating frequency estimates as these frequencies were not as well defined. This is because on a percentage basis slight variations in the strumming frequency correspond to large changes in the beating frequency. On an absolute scale, it can be said that the estimates listed are within 0.5 rad/sec based on the processed spectra.

The lowest beat frequency determined corresponded to the deepest instrument bottle, namely bottle A. The low-frequency spectra in figure 5-9 clearly show a strong peak at

DATASET	DEPTH (METERS)	STRU. FREQ. (ESTIMATE)	BEAT. FREQ. (ESTIMATE)
A	1200	33.2	0.25
B	1000	33.3	0.50
C	610	33.6	1.20
D	250	32.7	1.15
E	100	30.0	0.63

Table 5-III: Estimates of strumming and beating frequencies at discrete points along the cable

around 0.5 rad/sec. Remember that the processing techniques act to double the actual frequency value. For bottle B, however, the beat frequency was not as well defined as the two processing techniques seem to point to different values. The strong peak at 1.0 rad/sec determined from the envelope method and the existence of a similar peak in the homomorphic processed spectra yielded the chosen estimate. For bottles C and D some scatter did occur in the low-frequency range but dominant peaks were still identified. For bottle E the beat frequency seems fairly well defined at a value of 1.3 rad/sec.

The strumming frequency estimates are plotted in figure 5-14 along with the beat frequency estimate at each point. As readily seen, a high degree of shear exists over the upper half of the cable. As a result the beat frequencies tended to be higher in this region. Over the lower half of the cable very little shear occured and the determined beat frequency

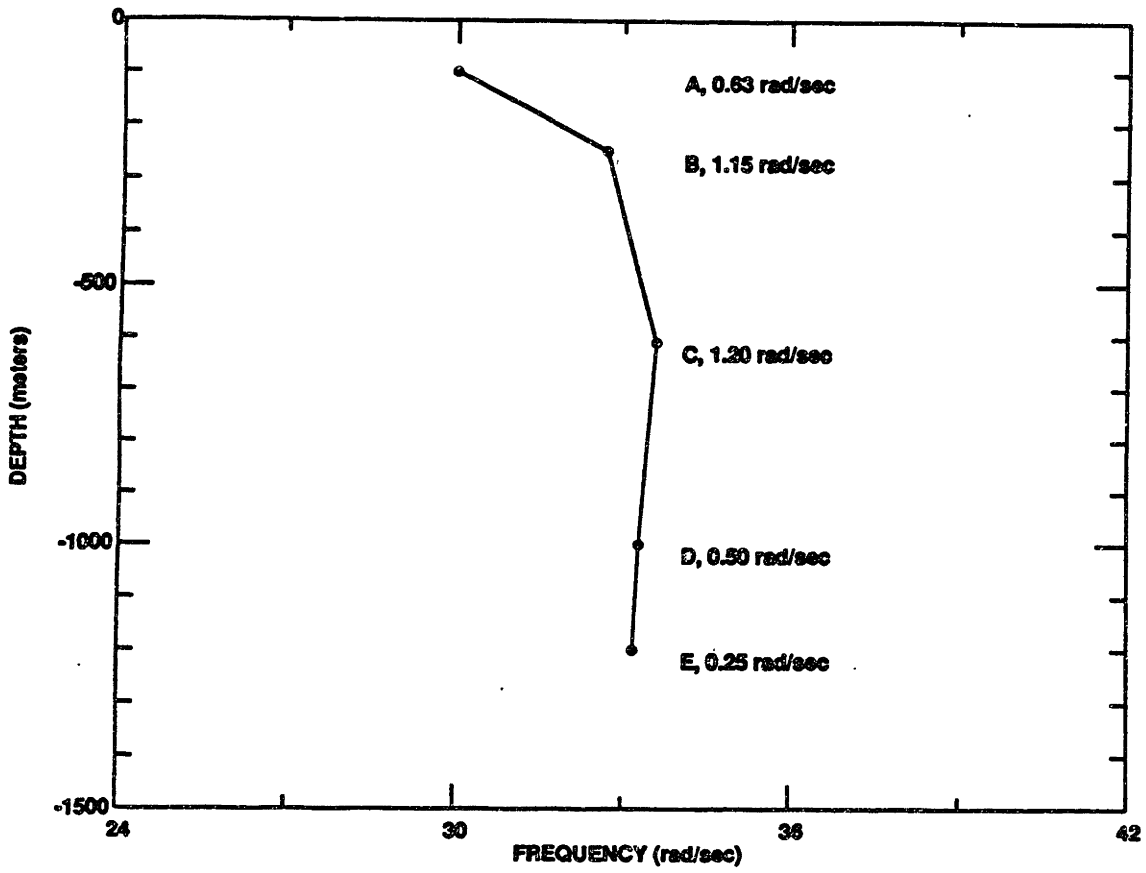

Figure 5-14: Variation of strumming and beating frequencies with depth

tended to decrease. In the numerical studies the beat frequency was determined to be dependent on the difference between the local and closest end point excitation frequency. This may provide some reasoning behind why the beat frequencies tended to increase toward the cable midpoint.

Chapter 6

Conclusions and Recommendations

The well known two-point excitation problem suggested that amplitude modulation of the vibration response should occur when the loading is continuous and exhibits some form of frequency variation along the cable length. This postulate was confirmed by the results obtained from the SCVP model. This model provides a relatively simple means by which the effects of problem parameters, such as damping, can be investigated. The results show a definite dependence on correlation length and damping as well as the shape of the current profile. Decreasing the correlation length tends to create a more random series of beats while increasing the damping past some critical value tended to eliminate beating all together. Additional research is required to more concretely define the extent to which these parameters effect the vibration response. The magnitude of the beat frequency was shown to dependent on the difference between the local and closest endpoint excitation frequencies for the case when the vortices were correlated along the entire length of the cable.

The two processing techniques presented in Chapter 5 have proven to be very effective tools in the frequency analysis of time series records. Both methods, homomorphic processing and the envelope approach, aided in the determination of the dominant beat frequencies. The long time series records proved to be useful in the spectral analysis as the requirements of spectral resolution and variance reduction could both be sufficiently satisfied. However, some scatter of results did occur from slight variations in the excitation over this long period.

The full-scale data confirms that the beat frequency is strongly dependent on the

excitation frequency gradient. The strong frequency gradient over the top half of the cable gave rise to larger beat frequencies. The beat frequencies tended to increase toward the center of the cable where the difference between the local and cable endpoint frequencies was a maximum. In addition, the strumming frequency was determined to be very close to the theoretical Strouhal frequency. The time series records exhibited beating that appeared fairly random in nature. This can be supported by the theoretical studies if one considers that in the full-scale test the vortices were not well correlated along the cable length.

References

[1] Ambramowitz, M., and Stegun, I.A.
Handbook of Mathematical Functions.
Dover Publications, Inc., 1972.

[2] Engebretsen, K.B.
An Analysis of Full-Scale Experimental Data On the Dynamics of Very Long Tethers Supporting Underwater Vehicles.
Master's thesis, Massachusetts Institute of Technology, February, 1988.

[3] Faltinsen, O.M.
Sealoads and Marine Operations.
September, 1986.
Class Notes.

[4] Kim, Y.H.
Vortex-Induced Response of Drag Coefficients of Long Cables Subjected to Sheared Flows.
PhD thesis, Massachusetts Institute of Technology, October, 1984.

[5] Koopman, G.H.
The Vortex Wakes of Vibrating Cylinders at Low Reynolds Numbers.
Journal of Fluid Mech. , June, 1987.

[6] Oppenheim, A.V., and Schafer, R.W.
Digital Signal Processing.
Prentice Hall, Inc., 1975.

[7] Press, W.H., Flannery, B.P., and Teukolsky, S.A., Vetterling, W. T.
Numerical Recipes.
Cambridge University Press, 1989.

[8] Sarpkaya, T.,and Issacson, J.
Mechanics of Wave Forces on Offshore Structures.
Van Nostrand Reinhold Co., 1981.

[9] Skop, R.A., Griffin, O.M., and Ramberg, S.E.
Strumming Predictions for SEACON II Experimental Mooring.
OTC 2884 , May, 1977.

[10] Welch, P.D.
The Use of the Fast Fourier Transform for Estimation of Power Spectra.
IEEE Trans. Audio Electroacoust. , June, 1970.